TKK Dissertations 84
Espoo 2007

APPLICATIONS OF FIBER OPTICAL RESONATORS IN MEASUREMENT AND TELECOMMUNICATIONS TECHNOLOGY

Doctoral Dissertation

Tuomo von Lerber

Helsinki University of Technology
Department of Electrical and Communications Engineering
Micro and Nanosciences Laboratory

TKK Dissertations 84
Espoo 2007

APPLICATIONS OF FIBER OPTICAL RESONATORS IN MEASUREMENT AND TELECOMMUNICATIONS TECHNOLOGY

Doctoral Dissertation

Tuomo von Lerber

Dissertation for the degree of Doctor of Science in Technology to be presented with due permission of the Department of Electrical and Communications Engineering for public examination and debate in Micronova at Helsinki University of Technology (Espoo, Finland) on the 5th of October, 2007, at 12 noon.

Helsinki University of Technology
Department of Electrical and Communications Engineering
Micro and Nanosciences Laboratory

Teknillinen korkeakoulu
Sähkö- ja tietoliikennetekniikan osasto
Mikro- ja nanotekniikan laboratorio

Distribution:
Helsinki University of Technology
Department of Electrical and Communications Engineering
Micro and Nanosciences Laboratory
P.O. Box 3500
FI - 02015 TKK
FINLAND
URL: http://www.micronova.fi/units/mns/
Tel. +358-9-4511
Fax +358-9-451 3128
E-mail: Tuomo.Lerber@iki.fi

ISBN 978-951-22-8901-1
ISBN 978-951-22-8902-8 (PDF)
ISSN 1795-2239
ISSN 1795-4584 (PDF)
URL: http://lib.tkk.fi/Diss/2007/isbn9789512289028/

TKK-DISS-2332

Multiprint Oy
Espoo 2007

ABSTRACT OF DOCTORAL DISSERTATION	HELSINKI UNIVERSITY OF TECHNOLOGY P. O. BOX 1000, FI-02015 TKK http://www.tkk.fi

Author	Tuomo von Lerber

Name of the dissertation
Applications of fiber optical resonators in measurement and telecommunications technology

Date of manuscript	April 10, 2007	Date of the final manuscript	August 27, 2007
Date of the dissertation	October 5, 2007		
☐ Monograph		☒ Article dissertation (summary + original articles)	
Department	Electrical and Communications Engineering		
Laboratory	Micro and Nanosciences Laboratory		
Field or research	Optical technology		
Opponent	Peter Andrekson, Professor		
Supervisor	Hanne Ludvigsen, Docent		

Abstract

The advent of optical fibers has greatly impacted the modern technology landscape. Most notably, existing telecommunications infrastructure relies on optical fiber networks, which have the ability to transmit high-bandwidth data over considerable distances. Optical fibers have also visible foothold in the field of metrology, where they are used as sensors in various applications.

An optical resonator is a basic building block of many optical devices, such as lasers, measurement probes, and optical signal processing equipment. In this dissertation we propose new methods and tools for metrology and general telecommunications sciences based on fiber optical resonators. Compared to conventional free-space technology, fiber resonators enable easy connectivity and they are shown to be robust against ambient perturbations.

This thesis consists of two parts that concentrate on optical measurement and signal processing technology, respectively. The first part introduces new measurement schemes for fiber loss and minute birefringence quantification. A loss of an optical fiber medium is measured using a so-called fiber cavity ring-down method. In presence of an external source of loss, such as fiber bending or degradation, one may obtain information about the environment of the probe. Another scheme measures birefringence and, thus, the beat length of a short fiber section. We also suggest a computational method for resonator photon lifetime (also called resonator time constant) extraction under noisy signal conditions. We demonstrate that the developed algorithm may yield meaningful results even when conventional methods fail.

The second part of the thesis deals with all-optical signal processing and temporal data synchronization. In a proof-of-principle experiment we perform an all-optical clock recovery for 21 parallel wavelength channels at two simultaneous data rates. The method relies on a birefringent optical resonator, whose transmission spectrum is used to filter carrier and sideband frequencies of return-to-zero-modulated data for multiple wavelength channels. In another clock recovery experiment we investigate the possibility to use sideband filtered signal, combined with a continuous wave light emitted at the carrier wavelength.

Keywords	Optical fiber, resonator, cavity ring-down, clock recovery, birefringence		
ISBN (printed)	978-951-22-8901-1	ISSN (printed)	1795-2239
ISBN (pdf)	978-951-22-8902-8	ISSN (pdf)	1795-4584
Language	English	Number of pages	72 + app. 46
Publisher	Micro and Nanosciences Laboratory, Department of Electrical and Communications Engineering		
Print distribution	Micro and Nanosciences Laboratory, Department of Electrical and Communications Engineering		

The dissertation can be read at http://lib.tkk.fi/Diss/2007/isbn9789512289028/

VÄITÖSKIRJAN TIIVISTELMÄ	TEKNILLINEN KORKEAKOULU PL 1000, 02015 TKK http://www.tkk.fi

Tekijä	Tuomo von Lerber
Väitöskirjan nimi Kuituoptisten resonaattoreiden sovellukset mittaus- ja telekommunikaatiotekniikassa	

Käsikirjoituksen päivämäärä	10.04.2007	Korjatun käsikirjoituksen päivämäärä	27.08.2007
Väitöstilaisuuden ajankohta	05.10.2007		
☐ Monografia		☒ Yhdistelmäväitöskirja (yhteenveto + erillisartikkelit)	

Osasto	Sähkö- ja tietoliikennetekniikan osasto
Laboratorio	Mikro- ja nanotekniikan laboratorio
Tutkimusala	Optinen teknologia
Vastaväittäjä(t)	Prof. Peter Andrekson
Työn valvoja	Dos. Hanne Ludvigsen

Tiivistelmä

Optiset kuidut ovat vaikuttaneet voimakkaasti tekniikan kehitykseen kahdenkymmenen viime vuoden aikana. Erityisesti tämä näkyy telekommunikaatiossa, jossa olemassaoleva kiinteä infrastruktuuri nojaa optisiin kuituverkkoihin. Optisten kuitujen erityisominaisuus on niiden kyky kuljettaa tietoa pitkiä etäisyyksiä suurella kaistanleveydellä. Optisia kuituja käytetään myös yleisesti mittaustekniikan eri anturisovelluksissa.

Optisia resonaattoreita käytetään laajasti hyväksi mm. lasereissa, mittausantureissa ja optisissa signaalinkäsittelylaitteissa. Tässä väitöskirjassa esitellään uusia kuituoptisiin resonaattoreihin perustuvia menetelmiä ja työkaluja mittaus- ja telekommunikaatiotekniikan tarpeisiin. Verrattuna perinteisiin vapaan tilan optisiin komponentteihin, kuituresonaattorit tarjoavat helpon käytettävyyden mm. liitäntöjen suhteen. Optiset kuidut ovat osoittautuneet myös verrattain epäherkiksi ympäristöhäiriöille, kuten tärinälle.

Väitöskirja koostuu kahdesta osasta, joista ensimmäinen keskittyy mittaustekniikan ja toinen telekommunikaatiotekniikan sovelluksiin. Ensimmäisessä osassa esitellään uusia mittausmenetelmiä kuidun häviön ja kahtaistaittavuuden mittaamiseen. Kuitumateriaalin häviö tai sen muutos mitataan ns. *"cavity ring-down"*-menetelmällä. Resonaattorin lisääntynyt häviö, johtuen esim. läpäisevyyden pienenemisestä tai kuidun taivutuksesta, voi antaa tietoa kuidun ympäristöstä. Toinen tutkittu menetelmä mittaa kuidun kahtaistaittavuutta ja siten kuidun jaksollista pituutta (engl. *beat length*). Väitöskirjassa esitetään myös uusi laskentamenetelmä resonaattorin aikavakion määrittämiseen kohinaisesta signaalista. Työssä kehitetty algoritmi antaa mielekkäitä tuloksia erittäin kohinaisesta signaalista silloinkin kun perinteiset laskentamenetelmät muuttuvat epätarkoiksi.

Väitöskirjan toinen osa käsittelee optista signaalinkäsittelyä ja vastaanotettavan datan ajallista synkronointia. Esitämme optisen kellonpalautusmenetelmän (engl. *clock recovery*), jolla voidaan käsitellä useita yhtäaikaisia signaaleja. Toiminta osoitetaan 21 rinnakkaiselle aallonpituuskanavalle ja kahdelle eri datanopeudelle. Menetelmä perustuu kahtaistaittavaan optiseen resonaattoriin, jonka transmissiospektriä käytetään useiden kanto- ja sivutaajuuksien yhtäaikaiseen suodattamiseen. Toisessa kokeessa tutkitaan kellonpalautusmenetelmää, jossa useita sivutaajuuksia suodatetaan optisella resonaattorilla ja suodatetut taajuudet yhdistetään niitä vastaaviin jatkuvan valon kantotaajuuksiin.

Asiasanat	Optinen kuitu, resonaattori, cavity ring-down, kellonpalautus, kahtaistaittavuus		
ISBN (painettu)	978-951-22-8901-1	ISSN (painettu)	1795-2239
ISBN (pdf)	978-951-22-8902-8	ISSN (pdf)	1795-4584
Kieli	Englanti	Sivumäärä	72 + liit. 46
Julkaisija	Mikro- ja nanotekniikan laboratorio, Sähkö- ja tietoliikennetekniikan osasto		
Jakelu	Mikro- ja nanotekniikan laboratorio, Sähkö- ja tietoliikennetekniikan osasto		

Luettavissa verkossa osoitteessa http://lib.tkk.fi/Diss/2007/isbn9789512289028/

Preface

This Thesis is a result of a journey that started in December 1999. Little did I know about the challenges, the amount of work, and the awaiting moments of joy and excitement that would take place when joining the group of Prof. M. W. Sigrist at ETH Zurich. If there has been one single decision that has influenced my life, then this has been it! I am very thankful to Prof. Sigrist for taking a chance with me and allowing me to pursue paths whose outcomes were far from obvious. The work was performed in collaboration with ABB Corporate Research (Switzerland) within the frame of the KTI project 5259.1 KTS, whom I gratefully acknowledge. I also want to thank Tekniikan Edistämissäätiö for the grant supporting early stages of this work.

During my time in beautiful Switzerland I had the privilege to accompany a group of bright individuals, such as Dr. Albert Romann, Dr. Markus Nägele, and Dr. Cornelia Fischer. Without the sparking moments of brainstorming with Albert, the content of this work would have been very different—if existing at all. When thinking of methods for liquid cavity ring-down experiments, he is the one who uttered the words: "How about doing it with an optical fiber?" Indebted I remain.

Unpredictability is maybe the most exciting characteristic of any scientific work. One starts a journey, albeit being unsure of the road, sometimes even about the destination. During my last few weeks in Switzerland, I observed curious "bumps" on my oscilloscope screen. Back in Finland, it took me a year and a half of busy evenings, and a hefty stack of blank papers to derive the mathematics and to explain the observations. These seemingly innocent undulations guided me onto new paths of telecommunications technology and optical signal processing. At this time I was employed by Asperation Oy, now demerged into Perlos Corporation. I want to express my deepest gratitude to my superiors, Mr. Joni Hietala and Dr. Jukka Ranta for accepting the disclosure of invention and allowing me to invest the time in this work. Paralleled to my employment in Asperation and Perlos, I also joined the group of Dr. Hanne Ludvigsen as a graduate student at the Helsinki University of Technology. I want to thank Hanne for her continuous support, encouragement, and many hours of advice when polishing and improving my remaining manuscripts, and eventually this Thesis. I have learned to know her as a person with a true passion for the advancement of science.

I want to thank Dr. Matthieu Legré and Dr. Ari Tervonen for their thorough review and suggestions of improvements of the Thesis.

Special thanks belong to Prof. Seppo Honkanen and Prof. Franko Küppers for companionship and countless hours spent on the phone and in the laboratory. Thank you for trusting me when I had nothing else but just a bag of ideas. I want to thank also Mr. Jesse Tuominen for the exciting and enlightening measurement sessions.

Preface

It is said that behind every great man is a great woman. I am less confident about myself, but I surely have been blessed with a great woman—my beloved wife Annakaisa. Thank you so, so much for standing with me throughout this work. To my children Milja, Elina, Julia, and Joonas—I love you. Luckily you have been developing faster than my scientific achievements.

And finally, praise to God who has provided all these wonderful people to help and guide me through the amazing journey. Thank you!!

Helsinki, August 8, 2007

Tuomo von Lerber

Contents

List of publications

This dissertation consists of an overview and the following five publications:

[P1] T. von Lerber and M. W. Sigrist, "Cavity-ring-down principle for fiber-optic resonators: experimental realization of bending loss and evanescent-field sensing," Appl. Opt. **41**, 3567–3575 (2002).

[P2] T. von Lerber and M. W. Sigrist, "Time constant extraction from noisy cavity ring-down signals," Chem. Phys. Lett. **353**, 131–137 (2002).

[P3] T. von Lerber, H. Ludvigsen, and A. Romann, "Resonator based measurement technique for quantification of minute birefringence," Opt. Express **12**, 1363–1371 (2004).

[P4] T. von Lerber, J. Tuominen, H. Ludvigsen, S. Honkanen, and F. Kueppers, "Multichannel and rate all-optical clock recovery," Phot. Techn. Lett. **18**, 1395–1397 (2006).

[P5] T. von Lerber, J. Tuominen, H. Ludvigsen, S. Honkanen, and F. Küppers, "Investigation of multiwavelength clock recovery based on heterodyne beats of sideband-filtered signal," Opt. Comm. **271**, 87–90 (2007).

Author's contribution

The scientific results presented in this dissertation have been carried out during the years 2000–2006 with three international parties: Laboratory for Laser Spectroscopy and Environmental Sensing at ETH Zürich (ETH), Fiber-Optics Group at the Micro and Nanosciences Laboratory at Helsinki University of Technology (TKK), and College of Optical Sciences at the University of Arizona (UA). The dissertation consists of an overview and five publications referred to as [P1–P5]. All the publications are the results of team work. The author has written the first manuscripts of all publications.

For publications [P1–P2], the author constructed the measurement setup, carried out the measurements, and performed the analysis at ETH. For publication [P3] the author performed the experimental work at ETH, and the analysis at TKK. For publications [P4–P5] the author participated in the initial experiments at TKK, and the final measurements at UA. The author is also responsible of the analysis of these two publications.

Other related publications to which the author has contributed

T. Lerber and A. Romann, "Fiber optic sensor with an optical resonator," European patent application EP1195582, filing date 9 October 2000 (2002).

T. von Lerber, "All-optical signal processing method and device," International patent application PCT/FI2003/000848, filing date 7 November 2003 (2005).

1 Introduction

Optical fibers are widely used, not only as a passive light transmitting media, but also as measurement probes and optical signal processing components in the fields of measurement and telecommunications technology. In order to construct a fiber based instrument, the optical material is intentionally exposed to external perturbations, or its frequency response is modified to contain specific regions of transmission, rejection, or loss. This can be realized, e.g., by use of a fiber optical resonator, whose transmission spectrum contains periodic regions of high and low transmission. In the time domain this is manifested by "slowness" that can be described as the light storing capacity of the resonator. A way to construct a fiber resonator is to use a set of mirrors at the opposing ends of the fiber. This dissertation studies applications of fiber optical resonators in measurement and telecommunications technology. The studied schemes are based on cavity ring-down sensing and optical clock recovery.

The cavity ring-down principle is a common spectroscopic tool for measurement of weak absorption of gaseous media [1]. In the cavity ring-down scheme a short pulse of light is injected into an optical cavity and its decay, i.e., the time constant is observed. The rate of decay alters, for example, due to a presence of an absorbing intracavity substance. The method has been extended to measurement of absorption of plasma [2] and condensed state media, such as liquids [3]. One approach to determine the absorption of a liquid is to insert a sample in a glass cuvette, whose plane-parallel mirrors are oriented in the Brewster angle. The cuvette is located inside the resonator and the light is transmitted through the sample [4]. An alternative method is to dispense the liquid on the surface of a highly transparent dielectric object. In this arrangement, the light does not propagate through the sample, but the field is absorbed through evanescent coupling of the frustrated total internal reflection [5]. The method has also been used with a polygonally shaped dielectric resonator, where the light is coupled into the ring via evanescent coupling [6]. A natural evolution of the scheme is to use optical fibers instead of the monolithic dielectric ring. The use of fiber medium allows measurement of other physical parameters, such as strain [7].

An elementary part of the cavity ring-down scheme is the analysis of the ring-down time constants. The simplest form of analysis is to record the decay and linearize the data with a logarithmic function. Should the original decay follow the pure exponential trajectory with negligible offset, the data points are transformed around a straight line whose slope can be determined with the least square method. Due to inclusion of noise and other possible distortions the least square fitting is prone to error and the computation is often accompanied with weight information [8]. The time constant determination is sometimes also performed by nonlinear fitting methods using, for instance, Levenberg-Marquard scheme [9].

Conventional telecommunications single-mode optical fibers exhibit always some birefringence due to imperfections of the fabrication process. When fibers are used as the optical medium of the resonator, the intrinsic birefringence results in two different path lengths inside the resonator and thus creates two orthogonal cavity modes. Sometimes the resonators are used to measure weak birefringence effects, such as mirror birefringence [10], due to enhanced effective path length the light interacts with the double refracting medium.

Clock recovery is a common operation performed in virtually every telecommunications system, where the receiver interprets the transmitter clock directly from the incoming stream of data. The optical clock recovery methods can be divided into two categories: self-pulsating and filtering schemes. A self-pulsating clock recovery device employs an electro-optical [11] or an all-optical oscillator [12] that is injection locked to the rate of the incoming stream of data. In filtering schemes the clock tones of the data spectrum are separated from the data. The filtering has been demonstrated with use of Fabry-Pérot resonators [13, 14], stimulated Brillouin scattering filters [15], and Bragg grating filters [16]. The Fabry-Pérot filtering has traditionally been performed with a resonator, whose free spectral range coincides with the data rate of the bit stream such that the carrier and the sideband frequencies of a return-to-zero (RZ) -modulated signal have been transmitted, while other content of the data have been removed. In principle, the Fabry-Pérot filtering offers an opportunity for multiwavelength operation, should the channel grid coincide with an integer multiple of the free spectral range of the resonator [17]. So far, such demonstration has not been presented, because in real-life telecommunications systems the channel grid separation frequency does not match the data rate. Clock recovery for two simultaneous wavelength channels has been demonstrated with use of Brillouin scattering [18] and parametrically amplified mode-locked fiber laser [19], and for four channels with use of an semiconductor optical amplifier (SOA) array module in a mode-locked fiber laser [20].

The first part of this dissertation discusses about fiber optical resonator based measurement technology and we introduce two new measurement schemes for quantification of fiber loss [P1] and birefringence [P3]. The first introduced method is so called fiber cavity ring-down method, which measures loss of an optical fiber medium. In presence of specified external source of loss, such as fiber bending or degradation, one may obtain information about the measured object or environment. The other introduced scheme measures birefringence and, thus, the beat length of a short fiber section. We also introduce a computational method for resonator time constant extraction under elevated noise conditions [P2].

The second part of the thesis focuses on all-optical signal processing and telecommunications technology. In a proof-of-principle experiment we perform an all-optical clock recovery for 21 simultaneous wavelength channels at two simultaneous data rates [P4]. The method relies on a birefringent optical resonator, whose transmission spectrum is used to simultaneously filter carrier and sideband frequencies of return-to-zero-modulated data for multiple wavelength channels. In another clock recovery experiment we investigate the possibility to use sideband filtered signal, combined with a continuous wave light emitted at carrier wavelength [P5].

2 Fiber optical resonator

Optical fibers have been employed in an abundance of fields and applications, ranging from optical telecommunications to measurement technology, and from material processing to illumination and decoration. In the field of telecommunications the optical fibers have been adopted as the preferred information carrying medium. Compared to alternative solutions, such as copper wires, optical fibers have superior capacity to carry vast amounts of data over prolonged distances. In fact, a single-mode fiber has unparallel bandwidth-distance product to most other solid-state media. Only free-space optical links may achieve similar performance, yet, with another set of limitations, which render them impractical for majority of terrestrial communications applications.

Sometimes fibers serve not only as a light transmitting medium, but they are used to construct optical devices, such as interferometers and sensors [21], filters [22], and lasers [23]. In this dissertation fibers are used to construct optical resonators. Fiber based resonators provide an excellent solution with ease of handling, ease of connectivity, and flexibility one may not achieve with conventional free-space resonators. Moreover, fibers are designed to be possibly immune to environmental effects. Therefore, changes in optical properties of a short fiber section are typically intentional and can be used to alter the resonator itself.

2.1 Fabry-Pérot resonator

Optical resonators are found in a variety of shapes and designs [24]. The simplest of them is a pair of plane-parallel mirrors, separated by some transparent optical medium, like vacuum, air, or glass (see Fig. 2.1). A resonator of this type has been known since the late 19^{th} century when Charles Fabry and Alfred Pérot published an article on a device nowadays called a Fabry-Pérot (FP) interferometer, a FP cavity, or a FP resonator* [25]. A FP resonator is rarely used in large free-space optical systems due to non-trivial alignment requirements. Even a slight misalignment or mechanical perturbation may cause the beam "walk off" the resonator, which translates into a severe alignment loss. Thus, the lack of transversal confinement in the free-space optical resonators implies a need to utilize mirror configurations, which support minimal transversal radiation. This is typically achieved with curved mirrors, which provide, e.g., Hermite-Gaussian solutions of the Helmholtz equation. Also other resonator forms exist, where the transmission medium and the number and shape of mirrors vary. In fact, resonators may be formed even without mirrors, such as ring resonators [26].

*The words "cavity" and "resonator" will be used interchangeably throughout this document.

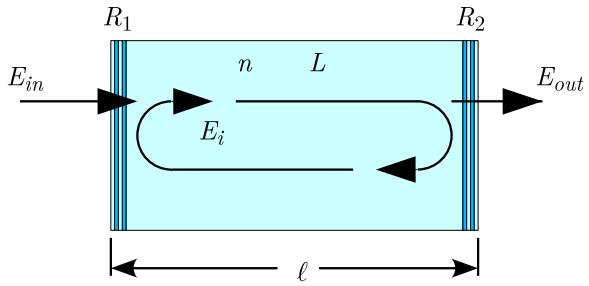

Figure 2.1: A model of a dielectric FP resonator. Symbols: E_{in}–incident electric field, E_{out}–output electric field, E_i–intracavity electric field, n–index of refraction, L–one-pass intensity loss, ℓ-length, and R_1 and R_2–intensity reflectivity of first and second cavity mirror, respectively.

An optical fiber may act as a resonator, once the confinement of light is not only transversal, but also longitudinal. The light may be "trapped" inside the fiber core when some form of reflecting mechanism is applied, which provides sufficient reflectivity and negligible absorbance. One example is a dielectric stack mirror, which may provide a reflectivity of >99%. Also metallic mirror coatings can be used, should the coated layer be thin and transparent enough. In addition to external coatings, optical fiber medium offers a possibility to use Bragg grating (FBG), which effectively forms an internal mirror for a particular wavelength of light [22].

2.2 Characteristics of optical resonators

Figure 2.1 depicts a dielectric FP resonator, where the light is confined in the core of a single-mode fiber, and two non-absorbing plane parallel dielectric mirrors with intensity reflectivity of R_1 and R_2 are facing each other at the opposing ends. The mirrors are separated by a distance of ℓ, and the intracavity optical medium has one-pass fractional intensity loss of L, and the index of refraction of n. An electric field $E_{in,0} = \sqrt{I_{in,0}}$ is incident to the first mirror at time $t = 0$, where $I_{in,0}$ is the intensity of light. A beam of light at a non-absorbing surface is partially reflected and partially transmitted, such that the intensity transmission $T_1 = 1 - R_1$. The electric field transmitted into the resonator is thus $E_0 = E_{in,0}\sqrt{1 - R_1}$. After the first round-trip at time $t = t_{rt} = 2n\ell/c$ the intracavity electric field has passed twice the optical medium, has leaked through both resonator mirrors, and has accumulated some phase shift such that the field may now be written as

$$E_1 = E_{in,1}\sqrt{1 - R_1} + E_0\sqrt{R_1 R_2}\,(1 - L)\exp(i\varphi)\,, \tag{2.1}$$

where $E_{in,1}$ is the field injected at time $t = t_{rt}$, round-trip phase shift $\varphi = 4\pi n\ell/\lambda$, and λ is the wavelength of light in vacuum. For succeeding round-trips the intracavity field may be generalized as

$$E_N = E_{in,N}\sqrt{1 - R_1} + E_{N-1}\sqrt{R_1 R_2}\,(1 - L)\exp(i\varphi)\,. \tag{2.2}$$

The electric field leaked through the second mirror is

$$E_{out,N} = E_N \sqrt{(1-R_2)(1-L)} \exp(i\varphi/2), \tag{2.3}$$

which finally provides the output intensity $I_{out,N} = |E_{out,N}|^2$.

The resonator transmission spectrum

$$T = \frac{I_{out}}{I_{in}} = \frac{(1-R_1)(1-R_2)(1-L)}{\left[1-(1-L)\sqrt{R_1R_2}\right]^2 + 4(1-L)\sqrt{R_1R_2}\sin^2(\varphi/2)} \tag{2.4}$$

can be calculated when the number of round-trips is approaching infinity under constant injection of input intensity I_{in} [24]. The transmission spectrum is a function of the round-trip phase shift φ with the period of 2π. When translated into the frequency of light, the free spectral range (FSR) is

$$\Delta\nu = \frac{c}{2n\ell}, \tag{2.5}$$

where c is the speed of light in vacuum.

The response of a lossless FP resonator is depicted in Fig. 2.2, where a pulse of light is injected into the cavity. The output intensity exponentially approaches the level of input intensity when the optical path length of the resonator is an integer multiple of the half-wavelength of light (solid line, phase shift $\varphi_1 = 0°$). The wavelength of light is matched with the optical length of the resonator. In this case a strong standing wave is accumulated inside the resonator, which leaks through both cavity mirrors. At the input side the out-leaked and the reflected electric fields interfere destructively and the resonator appears to have nil reflection for this particular wavelength of light. On the opposing side the out-leaked field equals with input field and the resonator gives an appearance of transparency.

When the wavelength of light is not matched with the resonator the accumulated intra-cavity field is complex-valued and no standing wave is formed. Depending on the amount of phase mismatch and the resonator bandwidth, some residual field is still accumulated with small and beating amplitude. In Fig. 2.2 this is illustrated with the dashed response line ($\varphi_2 = 15°$), which shows damped and oscillating output. With suitable selection of parameters and some amplification this ringing can, and will be used for practical purposes as discussed in Sections 5 and 6.

As noted earlier the output intensity exponentially follows the input; in other words there is a delay in the response. The resonator evidently has a memory of its past, which is already expressed in Eq. (2.2). The resonator time constant, which sometimes is referred to as the photon lifetime, can be written as

$$\tau = \frac{n\ell}{c}\frac{1}{|\ln[(1-L)R]|} = \frac{1}{2\pi\delta\nu}, \tag{2.6}$$

where

$$\delta\nu = |\ln[(1-L)R]|\frac{c}{2\pi n\ell} \tag{2.7}$$

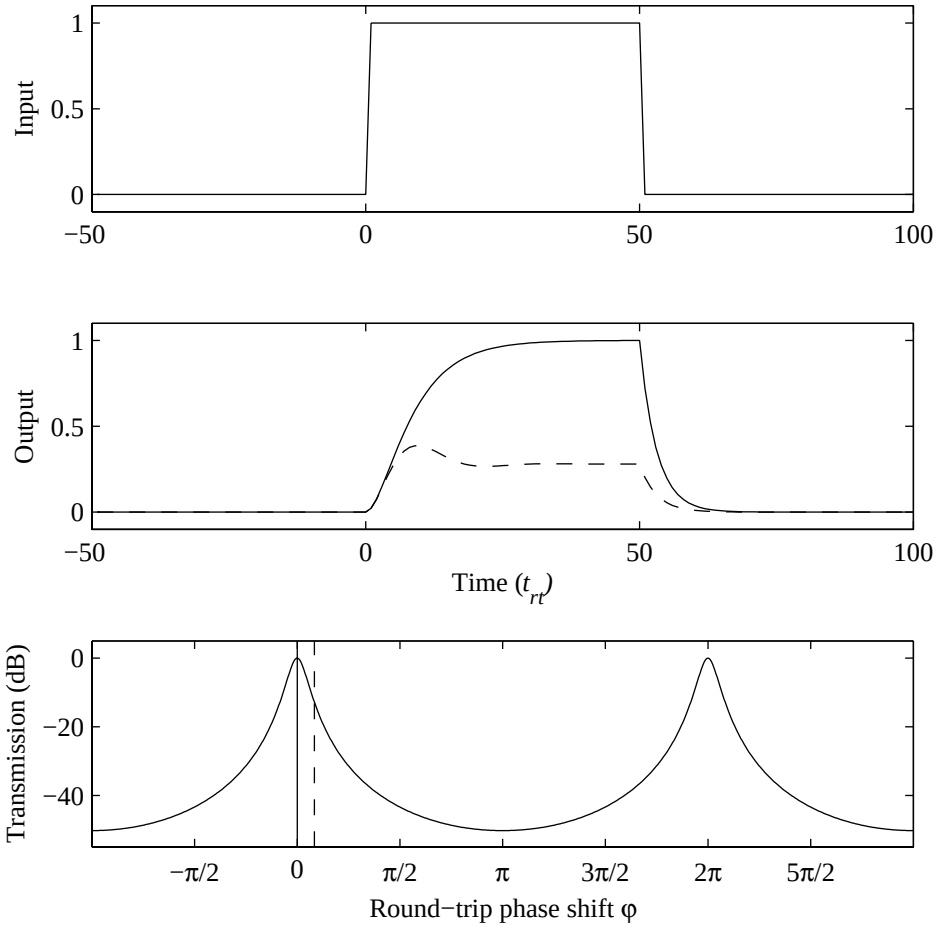

Figure 2.2: Simulated response of a lossless FP resonator ($R_1 = R_2 = 0.85$). Top: Incident input intensity. Middle: Resonator output for round-trip phase shift of $\varphi_1 = 0°$ (solid line) and $\varphi_2 = 15°$ (dashed line). Bottom: Transmission spectrum of the resonator. Locations of the phase shifts for calculated curves are marked with a solid and dashed line, respectively.

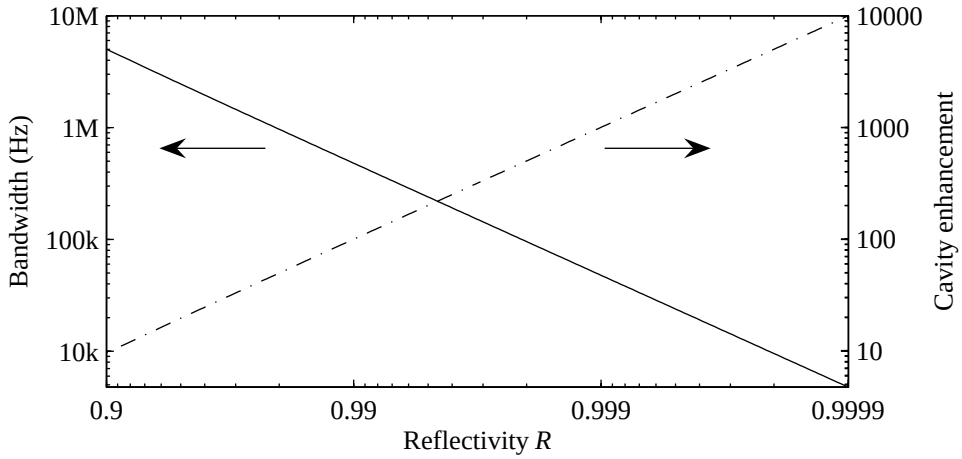

Figure 2.3: Bandwidth and enhancement factor of a lossless ($L = 0$) resonator with length ℓ of 1 m and an index of refraction n of 1.

is the full-width at half-maximum (FWHM) bandwidth of the transmission spectrum, and $R = \sqrt{R_1 R_2}$ is the geometric average of the cavity mirror reflectivity of R_1 and R_2. The cavity enhancement factor

$$\frac{1}{|\ln[(1-L)\,R]|} \approx \frac{1}{L+(1-R)} \quad (L \approx 0,\ R \approx 1) \tag{2.8}$$

in Eq. (2.6) represents the increase of intracavity intensity with respect to incident light at the wavelength of resonance. The enhancement factor could also be interpreted as an increase of effective path length a photon experiences due to resonance. The cavity enhancement and bandwidth are depicted in Fig. 2.3 for a generic resonator. The figure exemplifies well that cavity enhancement, and thus the photon lifetime, is inversely proportional to the transmission bandwidth of the resonator. A desire to have long photon life time yields in narrow bandwidth, which in real systems often complicates the in-coupling of light. In case of a very high-finesse cavity the in-coupling is notoriously difficult, when even a minor perturbation in emission wavelength results in beating or non-existent output signal.

3 Cavity ring-down principle for fiber optical resonators

The cavity ring-down (CRD) principle is a resonator based measurement scheme, commonly used to determine loss of an intracavity optical medium [1, 3, 8, 27]. The name "ring-down" is derived from the measurement event, where some light is injected into the resonator at the resonance frequency and the intensity of the light is quickly switched off. Accumulated intracavity intensity decays (rings down) and the rate of intensity decrease is monitored at the output. As has been shown earlier in Section 2.1, the rate of decay is strongly dependent on intracavity loss and can used to determine spectrum of the intracavity medium. Nowadays CRD spectroscopy has been adopted as the mainstream technology for sensitive direct absorption measurements of gaseous media.

In paper [P1] we present a variant of the CRD method based on fiber optical resonators. The use of fiber medium enables measurement of absorption, but also other physical parameters, such as structural deformation, degradation, or even electric current or magnetic field. In a proof-of-principle experiment the method is demonstrated for measurement of bending loss and evanescent field absorption.

3.1 Foundations of CRD principle

The CRD scheme is an absolute measurement technique for magnitude of loss of an optical resonator. When the effective reflectivities of the resonator mirrors are known (including the cavity medium and mirror scattering losses) the absolute transmission loss caused by an additional source can be directly determined.

A ring-down event is invoked when a pulse of light is injected into an optical resonator, typically a free-space optical cavity (see Fig. 3.1). The intracavity intensity will gradually decrease due to imperfect reflections and losses of the cavity medium. Ideally, the intensity decay adopts the form of a monoexponential function $I = I_0 \exp(-t/\tau)$, where I_0 is the intensity of light at time $t = 0$, and τ is the resonator time constant. The time constant τ will change, when any parameter of Eq. (2.6) is varied. For example, when an absorbing substance is inserted into the cavity the time constant can be written as

$$\tau_1 = \frac{n\ell}{c} \frac{1}{|\ln[(1 - L - \Delta L)\, R]|} \approx \frac{n\ell}{c\,[L + \Delta L + (1 - R)]}, \tag{3.1}$$

where ΔL is the increase of loss. The approximation is valid when reflectivity is close to unity ($R \approx 1$), and the loss and its increase are small ($L \approx \Delta L \approx 0$). The magnitude

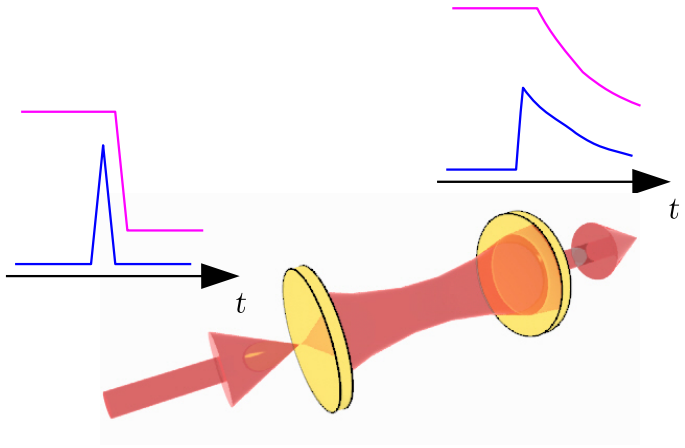

Figure 3.1: CRD method. After a short pulse (blue line) or a rapid switch-off of CW light (magenta line), the output intensity of a resonator decays exponentially.

of the time constant change is higher, the higher the reflectivity R and the lower the initial loss L are. As discussed in [P1] and [28] the relative time constant sensitivity is obtained with partial derivation

$$\frac{\Delta\tau}{\tau} = \frac{1}{|\ln\left[(1-L)\,R\right]|}\left[\frac{\Delta R}{R} - \frac{\Delta L}{(1-L)}\right]. \tag{3.2}$$

The CRD principle has several benefits over conventional direct absorption measurement, which is based on determination of transmission intensity difference. Namely, instead of measuring the actual absorbance the CRD method measures the *rate* of absorbance. For this reason the method is insensitive for light source intensity fluctuations. Another benefit of the method is the high sensitivity in case of a high-finesse cavity, which provides long effective path lengths. For example, a lossless 1 m long resonator with mirror reflectivity of 99.99% translates into an effective e^{-1} path length of 10 km.

3.2 History and development of CRD spectroscopy

The CRD method was originally developed for measurement of high-reflectivity mirrors, which were difficult to characterize otherwise [1, 29, 30]. For example, measurement of mirror reflectivity of 99.9% is inherently difficult, because the reading of intensity difference of 0.1% must be made against enormous background of light. This would require ultra-stable light source, photo detectors, and amplifying electronics. Therefore, measurement of the time constant instead of the intensity is highly desirable.

The CRD spectroscopy was invented when O'Keefe and Deacon introduced in 1988 a new spectroscopic tool based on pulsed light sources [31]. Since then numerous of works, especially in the fields of chemical physics and spectroscopy have used or further developed the method.

Early works in the field of CRD spectroscopy used pulsed laser sources [31–33], which provide a natural "switch-off" of the light. However, this approach suffers several drawbacks. Namely, the output intensity is often small due to weak in-coupling and the linewidth of the pulse is easily limiting the spectral resolution. In the vicinity of strong narrow-band absorption the output transient is necessarily no more monoexponential and the signal may contain contribution from several time constants. Also, when the pulse linewidth exceeds the FSR of the resonator, the output exhibits a beating signal due to longitudinal multimode excitation [34].

An obvious solution for these problems is to use a narrow linewidth CW source combined with an external modulator for rapid intensity switch-off [35]. A challenge of this approach is the locking of the light source and the cavity modes. In particular, a short term frequency jitter exhibited by many CW sources is easily larger than the bandwidth of a high-finesse resonator.

In practical setups no permanent locking is achieved, nor attempted. Cavity length is slowly swept with, e.g., piezoelectric transducer and once the buildup occurs the light is rapidly switched off with a modulator [35]. Alternatively, the resonator length may be changed suddenly such that no in-coupling occurs [36]. Still another approach is to keep the cavity stable (or unregulated) and to sweep the wavelength of light [37]. In our experimental setup we used a combination of these approaches. We swept the wavelength of light, but the switch-off was made by directly modulating the laser source [P1].

In the early days of the development of the CRD scheme there were confusion about the nature of coherence effects in high-finesse cavities. It was argued that a short pulse of light may be absorbed by intracavity narrow-band absorption, which falls outside of resonator transmission modes. This prompted a series of papers, which addressed the misunderstandings [34, 38, 39].

Cavity ring-down spectroscopy, which was initially developed for the measurement of gaseous media in free-space cavities, has evolved in new directions. For example, a broadband nature of a dye laser and its multi-mode excitation were successfully used to perform Fourier transform interferometric CRD experiments [33]. Also, the CRD principle, which originally was developed for measurement of gaseous media, has been extended to measurement of liquids [4, 40]. Recently, the method has been extended into the direction of evanescent field sensing using dielectric resonator medium [5, 6, 41–43]. It differs from free-space cavity approach such that the interaction of light with the absorbing substance does not occur in "normal" transmission, but via evanescent field of the total internal reflection. A possible evanescent field CRD setup is depicted in Fig. 3.2. In general, evanescent field CRD systems could be seen as a precursor for fiber based CRD methods.

3.3 Cavity ring-down sensing with optical fiber medium

The intention was to study new sensitive spectroscopic methods for bio-chemical sensing of liquid samples, which could be used, for instance, to detect certain trace hormones

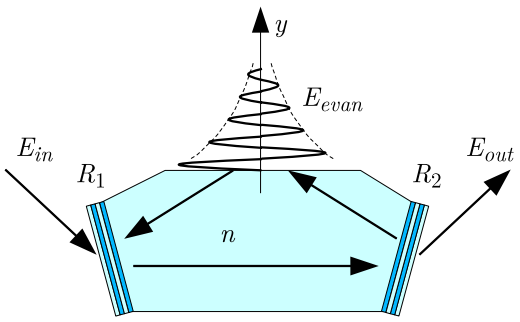

Figure 3.2: A schematic illustration of a possible evanescent field CRD setup. Symbols: E_{in}–incident electric field, E_{out}–output electric field, E_{evan}–evanescent field, n–index of refraction, y–penetration depth, and R_1 and R_2–intensity reflectivity of first and second cavity mirror, respectively.

from saliva. Because the aim was to construct a field-deployable setup, some highly sensitive schemes, such as fluorescence spectroscopy were found inappropriate. Within the boundaries of high sensitivity and simplicity the CRD spectroscopy and especially the evanescent field experiments by Pipino *et al.* [6] were found interesting. The approach was developed further such that the polygonal dielectric resonator was replaced with an optical fiber [28].

Single-mode optical fiber is almost an ideal material base for an optical resonator. It is cheap, it has low transmission loss, and it is easy to handle and connect. For example, optical loss of commonly used Corning® SMF-28™ single-mode fiber is about 0.3 dB/km at the wavelength of 1550 nm, which is among lowest in all known solid state media. Another benefit of this particular breed of fibers is the ability to support only a single mode in the fiber core. As discussed in Section 3.2 multiple transversal modes often result in a beating output, and the ring-down envelope may not be monoexponential. By use of single-mode fibers this problem is virtually non-existent. Single-mode fibers are commonly used in telecommunications technology and fiber compatible equipment are readily available.

The scheme was demonstrated with fibers whose connectorized end-facets were coated with high-reflectivity dielectric mirrors [P1]. The feasibility was tested with bending and evanescent field absorption measurements. The method is suitable not only for measurement of absorbing media, but also other physical parameters.

The fiber CRD was introduced for the first time in 1988 by Morkel *et al.* who used the CRD scheme to measure the loss of a fiber laser medium [44]. Next time the subject emerged in 2001 by Stewart *et al.* who investigated an amplified fiber loop, which contained a micro-optic gas cell [45]. The amplification was required to compensate high coupling losses of the measurement cell. Although the idea is appealing, its realization proved to be non-trivial due to insufficient accuracy in gain control.

Since the publication of our work a number of new attempts have emerged, where the fiber CRD method has been developed further [46–48], or has been used for sensing of chemical [49–51], or physical parameters [7, 46, 52–55].

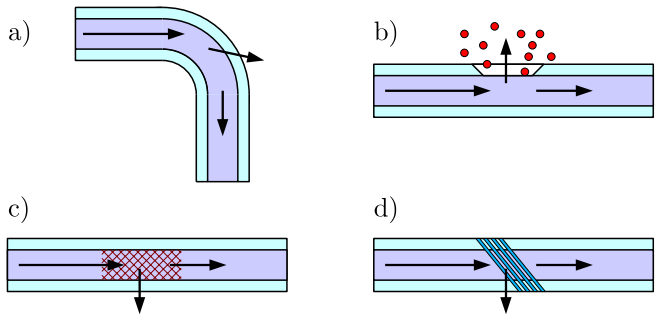

Figure 3.3: Examples of possible fiber loss mechanisms: (a) bending, (b) evanescent field absorption, (c) degradation, and (d) tilted Bragg grating.

Optical fiber CRD method has its own set of benefits and challenges. The benefit of the method is the high sensitivity, and possibility to measure virtually any physical parameter that may affect the loss properties of the fiber medium (see examples of Fig. 3.3). The challenge of the scheme, especially in conjunction of chemical sensing, is the issue of contamination. The evanescent field penetration depth is typically just few hundreds of nanometers, depending on the index difference of the exposed core and the external optical medium. Obviously, even an infinitesimal layer of contaminant may induce a gross error. This single factor may render the scheme impractical for routine use in field environment.

An interesting characteristic of fiber CRD scheme is the birefringent nature of the fiber medium, as discussed by Refs. [P1] and [46]. Two uneven effective path lengths inside the cavity create two separate orthogonal cavity modes. A high-finesse cavity fiber medium thus operates as a polarization selective element. The phenomenon and the applications of birefringence in conjunction with fiber resonators are discussed in more detail in Sections 5 and 6, and in publications [P3] and [P4].

3.4 Attempted measurement of Faraday effect

The paper [P1] claims that the fiber CRD method may provide means to measure a variety of physical parameters, including electric current or magnetic field. The claim was based on a novel work of R. Engeln *et al.* [56], who measured magneto-optic rotation of polarization in gaseous and solid media. We intended to utilize the same principle for optical fibers, whose Verdet-constant is well-known. The quantified magneto-optic rotation would be a direct measure of magnetic field, which in turn could be linked to the electric current.

We constructed a setup (see Fig. 3.4), where a copper wire was coiled around a fiber resonator whose output was directed to a polarizing beam splitter. The setup should have altered the time constants in the presence of magnetic fields, following the example of Ref. [56]. This did not happen although the applied magnetic field should have caused substantial rotation of polarization in our geometry and the change of time constant

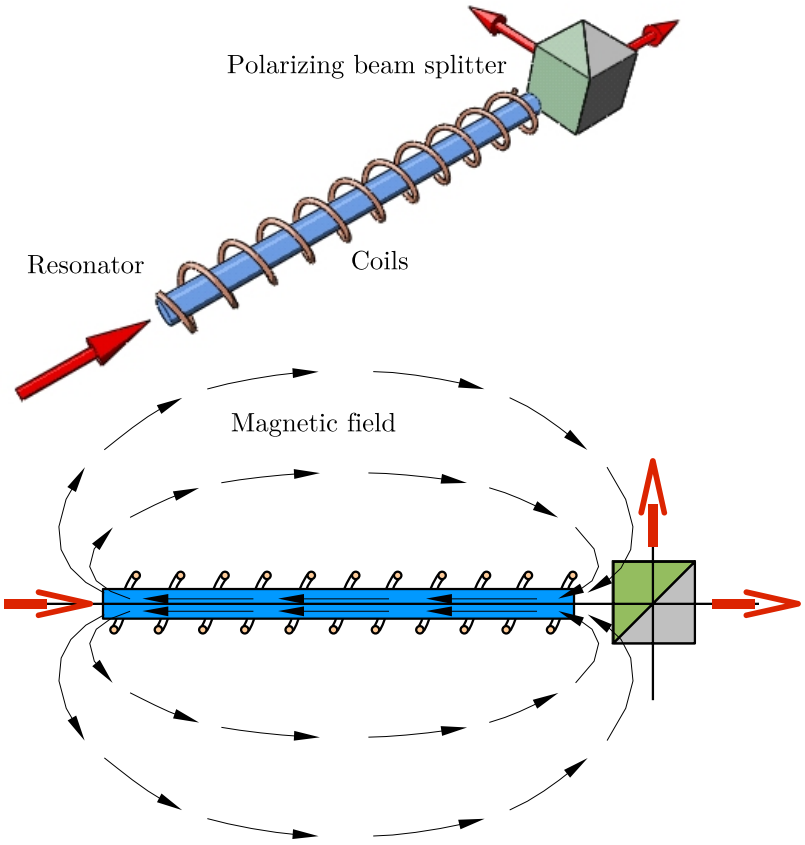

Figure 3.4: Schematic illustration of the attempted Faraday effect measurement setup.

should have been observable. The time constant of the ring-up and ring-down signals remained unchanged regardless of the presence or absence of the magnetic field.

The desired effect was absent, because the measurement geometries of Ref. [56] and ours consisted unexpected differences. In the setup of Ref. [56] the cavity length was about 50 cm and the duration of an optical pulse was about 5 ns, which translates in the pulse length of about 1.5 m and less than 4 complete intracavity round-trips. In case of a high-finesse cavity this means minimal accumulation of light and the input pulse may be perceived as an impulse function. Because of negligible self-overlapping of the intracavity pulse the light did not have to fulfill the resonance condition. In our setup the resonator length was about 60 cm and the pulse duration was about 500 ns, which inside the fiber medium translates into the pulse length of 100 m and 160 accumulated round-trips (resonator time constant was also about 500 ns). In other words, our signal overlapped itself so many times that the resonance condition had to be fulfilled.

Polarization properties of an intracavity optical medium, such as an optical fiber, can be represented by a Jones-matrix. The eigenvectors of the matrix mark the states of polarization, which, after a single cavity round-trip, return to their initial state.* In

*The Ref. [57] states that:

"... the eigenpolarizations of a birefringent Fabry-Perot resonator are always linear. The

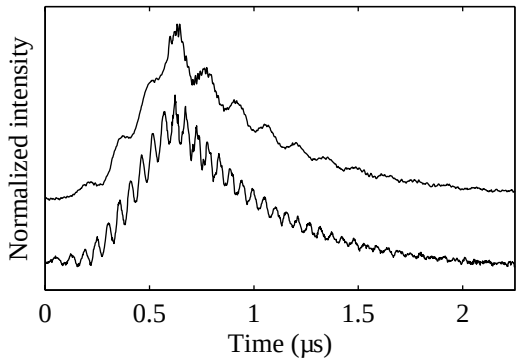

Figure 3.5: Two examples of beating ring-up and ring-down signals. The frequency of the beat is dependent on the amount of twist of the fiber resonator.

other words, only eigenpolarized light may fulfill the resonance condition, which, in turn, results in an unchanged time constant. We may conclude that the method of Ref. [56] implicitly requires a pulse of light, which approximates the impulse function.

Instead of observing a change in the time constant, an unexpectedly beating signal was recorded (see Fig. 3.5). Closer investigation revealed that the phenomenon was not related to the magnetic field, but was relying on the presence of the polarizing beam splitter. Also, the beat frequency appeared to be dependent on the fiber twist. We had not observed this type of beat earlier. Even more, it appeared that the phenomenon had no explanation within the framework of existing CRD literature. The origins of the beat are elaborated in Section 5 and in publication [P3].

azimuth of these linear eigenpolarizations might be different at the input and at the output of the cavity. However, as soon as there is some nonreciprocal optical activity (i.e., Faraday rotation) in the cavity, the eigenmodes become elliptical."

4 Time constant extraction

Determination of the time constant of an exponential decay is an integral part of any CRD experiment. In publication [P2] we discuss a few methods to extract the time constant and present a new one, which is proven to yield meaningful results under elevated noise conditions. The method is based on the weighted least square (WLS) method and Newton iteration with predefined minimum signal offset.

In general the temporal evolution of intensity of a CRD experiment is assumed to follow an exponential decay

$$I = I_{off} + I_0 \exp\left(-t/\tau\right), \tag{4.1}$$

where I_{off} is the signal offset intensity, I_0 is the intensity of light at time $t = 0$, and τ is the time constant. When the offset intensity I_{off} is zero, the time constant can be obtained by linearizing Eq. (4.1), which is written as

$$\ln I = \ln I_0 - \frac{t}{\tau}. \tag{4.2}$$

Once the exponential signal has been transformed into the logarithmic space, the time constant can be obtained from the slope (see Fig. 4.1). In an overdetermined system (with n data points and only one resolved variable) the computation is typically performed using the linear least square method. Despite the apparent simplicity of this approach the result may be erroneous due to distorted and noisy signal. The error is typically caused by increased uncertainty at the tail of a decay (see Fig. 1 in [P2]). A simple linear least square fit assumes equal weight for each data point and the degraded part of the signal erroneously contribute the calculation. Also, rejection of negative values in the

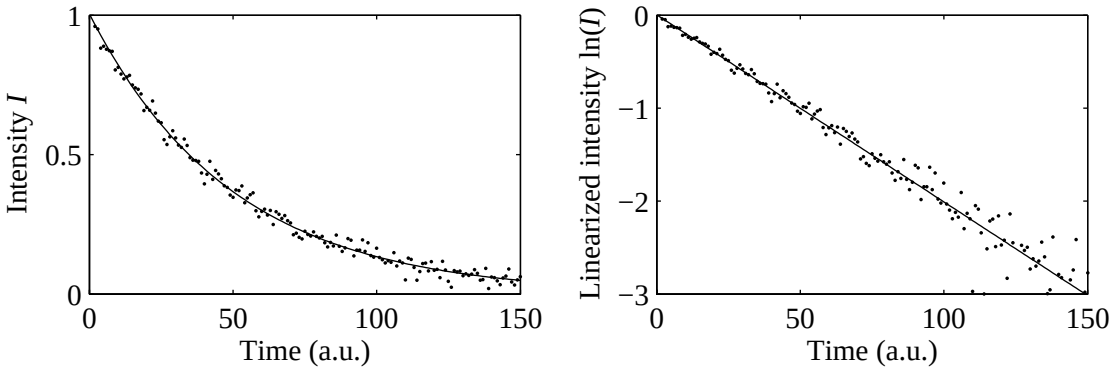

Figure 4.1: Simulated exponential decay ($\tau = 50$) in (left) linear and (right) logarithmic scale. The time constant τ is obtained from the slope of the linearized curve.

linearization will distort the result. For these reasons the linear least square method is often accompanied by weight information [3, 8, 42], which takes the predicted reliability of data points in account. As discussed in [P2] the WLS fitting has been proven to be a reliable and computationally efficient method.

4.1 Nonlinear fitting methods

In addition to linear least square fitting the time constant information can be obtained by using an iterative nonlinear algorithm, such as Levenberg-Marquard method [3,9,43]. In publication [P2] we introduce a nonlinear WLS method based on Newton iteration, where the linearization is performed through Taylor-series and an intentional offset is added to the signal. We show that our scheme imitates the conventional linear WLS method in a low-noise environment and a nonlinear fitting under high-noise conditions. Our scheme is shown to combine the good qualities of linear and nonlinear methods, benefiting from the existence of the weight matrix, but without the loss of information when the noisy decaying signal reach negative values. The WLS and Newton methods are shown to perform equally well in "normal" noise environment. Under excessive noise conditions the WLS algorithm is shown to become unpredictable while the Newton iteration retains its reliability. The introduced Newton algorithm requires more computational power than the WLS, but according to Ref. [3] less than Levenberg-Marquard method. Our scheme is believed to find applications in mid- and far-infrared CRD spectroscopy, where the photomultipliers or other high sensitivity detectors are not available.

4.2 Common assumptions in time constant extraction

In the following we briefly review two common assumptions associated with time constant determination. Their understanding bears substantial importance, because many schemes share the same assumption-base and ignorance may lead to highly erroneous interpretation of measurement data.

The most common assumption, used also in our discussion above, is the monoexponentiality of the decay (see Eq. (4.1)). This is true when a single transversal mode of a cavity is excited, e.g., in a single-mode fiber medium, *and* the emission bandwidth is narrower than the FSR of the resonator. For free-space optical cavities and pulsed laser sources this is necessarily not the case. When multiple cavity modes are excited, the CRD decay envelope becomes

$$I = I_{off} + I_0 \left[\exp\left(-t/\tau_1\right) + \exp\left(-t/\tau_2\right) + ... + \exp\left(-t/\tau_n\right)\right], \tag{4.3}$$

where τ_i, $(i = 1..n)$ is the time constant of one particular cavity mode. In the vicinity of a narrow-band resonance (compare Eqs. (4.1) and (4.3)) this assumption may result in an erroneous estimate for the time constant. The assumption of monoexponentiality is also used in our work [P2].

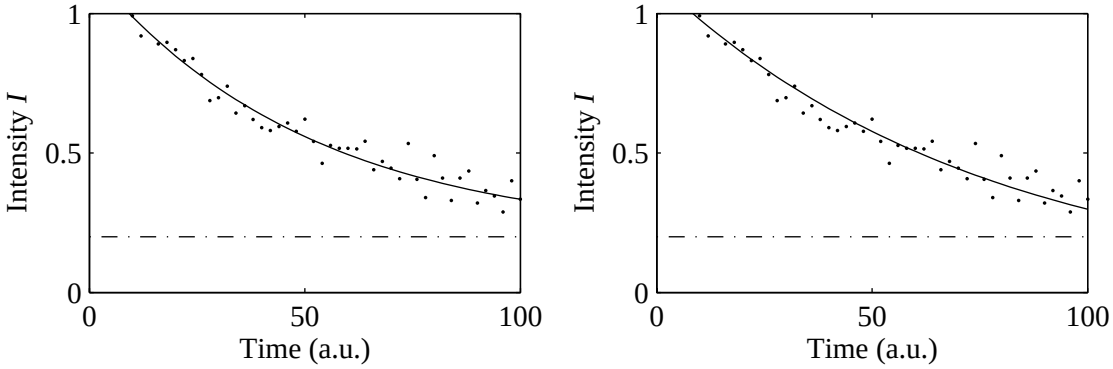

Figure 4.2: Effect of an uncompensated offset error. Simulated noisy decay (dots, $\tau = 50$), offset level (dash dotted line), and two fits are shown. The first fit (left, $\tau_1 = 50.1$) and the second fit (right, $\tau_2 = 74$) yield in different results due to compensated and uncompensated offset levels, respectively.

Another common assumption is the vanishing small, or properly compensated offset intensity ($I_{off} \approx 0$). This assumption deserves special attention, because even a minor uncompensated signal offset may become an influential source of error. The effect is simulated in Fig. 4.2, which depicts simulated noisy decay and two possible WLS fits. The fitted curves appear to model the decay sufficiently well although the derived results suggest otherwise. The difficulty of signal offset inaccuracy is that it remains easily unnoticed when the data acquisition time is less than 2τ. Therefore, the acquisition period should be long enough, or the offset information should be obtained by other means. The error and possible compensation methods are discussed in greater detail in Refs. [9, 58].

5 Quantification of minute birefringence

In publication [P3] we propose a highly sensitive measurement scheme to determine birefringence. The method is based on homodyne beats of polarized resonator output, which are directly proportional to the amount of birefringence. The scheme is demonstrated by measuring stress-induced birefringence of a twisted single-mode fiber.

5.1 Introduction to optical birefringence

Birefringence is a phenomenon of anisotropic optical media, where the index of refraction is dependent on the direction and the state of polarization of propagating light. The effect is often demonstrated with a calcite crystal located on top of an opened book. The birefringence splits the underlying text into two sets of partially overlapping images. The phenomenon has probably been known and utilized already in ancient times. For example, the Vikings have been claimed to use the "sunstones" (crystal cordierite) for maritime navigation, yet, the theory has recently been challenged due to lack of archaeological evidence [59]. The governing physical laws behind the double refraction were qualitatively explained in 1690 by the famous Dutch scientist Christiaan Huygens in his book *Traité de la Lumière* [60].

In many optical systems the birefringence is an undesired, often omnipresent parasitic effect. Birefringence of optical fibers in telecommunications systems causes polarization mode dispersion, or distorts the signal in integrated optical components. On the other hand, in some fields of measurement and display technology the birefringence is an elementary part of the working principle, such as in some measurement apparatus and liquid crystal displays, respectively.

The birefringence is present with varying degree, or can be made existent, in all dielectric media—even in vacuum [61]. Optical fibers are no exception. Imperfections in the fiber fabrication process always result in some geometric deformations of the fiber core, causing linear birefringence. Optical telecommunications links exhibit also circular birefringence due to twists of the installed fiber. The birefringence may also be induced by external perturbations, such as stress or bend. The complex evolution of polarization in the fiber was described already several years ago [62], but the subject matter continues to draw attention still today [63]. The on-going motivation to study the fiber polarization properties has been the increasing demand for high-speed optical networks, whose current bottleneck is the polarization mode dispersion. The polarization properties of fibers are also of keen interest in the development of fiber-optic resonator based devices, such as fiber lasers [64], and measurement instruments [46, 57].

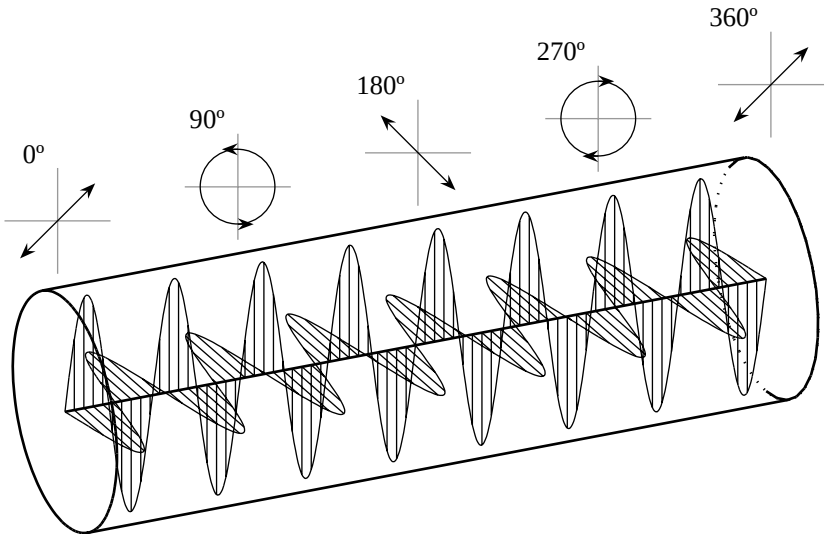

Figure 5.1: State of polarization evolves periodically in linearly birefringent fiber.

The degree and orientation of birefringence varies arbitrarily along the fiber. Therefore, the propagating electromagnetic field couples randomly to the two polarization modes, causing continuous variation in the state of polarization. Figure 5.1 depicts the evolution of polarization in a linearly birefringent fiber when both modes are evenly excited. As presented in the figure, after some distance the two propagating modes have accumulated a phase difference of 2π and the light has evolved back to its original state of polarization. This distance is called the beat length $L_B = \lambda/\Delta n$, where λ is the wavelength of light and Δn is the difference of the refractive indices of the polarization axis.

Circular birefringence is caused by chirality of some type of optical fiber medium, such as longitudinal twist. In other optical media the circular birefringence is typically caused by the presence of chiral material structures or molecules. The phenomenon may also be affected by the magneto-optical Faraday effect. The circular birefringence rotates the state of polarization such that its ellipticity is retained. For example, linearly polarized light in circularly birefringent medium stays linearly polarized, only the azimuth of the polarization vector is rotated. In historical and some contemporary texts the circular birefringence is referred to as the "optical activity".

5.2 Improvements of optical birefringence measurement

A conventional way to measure birefringence is to propagate a linearly polarized light through an optical medium such that its both states of polarization are excited, and to filter or split the output with a high extinction-ratio polarizer or polarizing beam splitter. The measured output intensity at the crossed state of polarization is proportional to the imposed ellipticity. While the degree of ellipticity depends on the interaction length in the doubly refracting medium, resonators are sometimes used to enhance the effect (see the discussion of resonator enhancement factor in Section 2.1). For example, low-birefringence phenomena, such as the Cotton-Mouton effect [65], and the attempted

measurements of vacuum birefringence [66] have been studied in high-finesse optical resonators.

The increase of effective path length enhances the measurement sensitivity, yet, this type of arrangement bears a particular set of challenges. For example, the in-coupling of light into a high-finesse cavity is non-trivial due to narrow resonance bandwidth. Additionally, the measurement result may be distorted by parasitic birefringence of the cavity mirrors. While the cavity arrangements are sensitive for parasitic mirror properties, it is not surprising that resonators are sometimes used for mirror birefringence characterization [10, 67–69].

Furthermore, the accuracy of the measurement can be improved by mixing a coherent local oscillator $E_1 \exp(i\omega_1 t)$ with a signal oscillator $E_2 \exp(i\omega_2 t + i\phi)$, which yields in the beating intensity

$$\begin{aligned} I &\propto |E_1 \exp(i\omega_1 t) + E_2 \exp(i\omega_2 t + i\phi)|^2 \\ &= E_1^2 + E_2^2 + 2E_1 E_2 \cos(\Delta\omega\, t + \phi), \end{aligned} \tag{5.1}$$

where ϕ is the phase shift, $\Delta\omega = |\omega_1 - \omega_2|$ is the difference of the angular frequencies of ω_1 and ω_2, and E_1 and E_2 are the amplitudes of the local and the signal oscillators, respectively. The magnitude of the intensity beat depends on the amplitudes of E_1 and E_2. When the signal oscillator intensity $I_2 \propto |E_2|^2$ is close or below the noise floor, the beating term may still provide data about the signal oscillator, because it has been amplified by the strong local oscillator. When the angular frequency difference $\Delta\omega = 0$, and the phase shift $\phi(t)$ is dependent on time, the scheme is called homodyne detection. When the angular frequency difference $\Delta\omega$ is non-zero the scheme is called heterodyne detection.

5.3 Homodyne beats of polarized resonator output

As discussed in Section 3.4 we observed unexpectedly beating ring-up and ring-down signals at the polarized fiber resonator output (see Fig. 3.5). The frequency of the beat was related to the orientation of the fiber and the data was recorded while gradually twisting the resonator. It is known that the twist of a fiber medium induces birefringence and creates two orthogonal polarization modes inside the resonator [62, 64, 70]. In publication [P3] we show that the two resonator modes create a homodyne beat when the output is polarized. We propose the method for high-sensitivity measurements of birefringence. The sensitivity of the scheme was demonstrated by measuring polarization properties of a 0.275-m long single-mode fiber resonator. The maximum beat length L_B of the fiber was found to be 10.6 m, which is almost 40 times longer than the length of the studied fiber itself. A measurement of fiber birefringence with a ratio of similar magnitude (L_B/fiber length = 14) has been demonstrated by Kuzin *et al.* [71].

The mathematical framework of publication [P3] is based on time-domain analysis, where the amplitude and phase of an electric field are expressed with phasor formalism. Mathematically phasors may be perceived as vectors, and accumulation of electric field inside

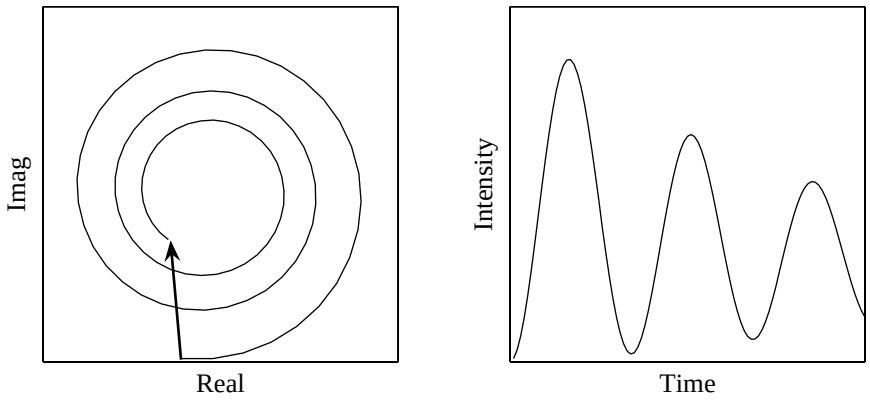

Figure 5.2: Phasor diagram (left) and output intensity (right) of a non-matched ring-up sequence. The square length of the sum vector equals with signal intensity.

the resonator is just a vector summation of complex numbers (see Fig. 5.2). The phasor formalism offers an opportunity to compute exact temporal evolution of the signal, as we did in our work (see, e.g., Fig. 5 in [P3]). This formalism is, however, not very intuitive when the input signal period approaches the round-trip time of a resonator.

The intracavity birefringence creates two orthogonal polarization modes and dual comb transmission spectrum as illustrated in Fig. 2 of publication [P1]. When light is injected at the resonance wavelength of one polarization mode (i.e., the wavelength of light is matched with the optical path length of the mode), some residual power will circulate in the other (non-matched) mode. The power oscillates in this non-matched mode, especially at the beginning of the ring-up and the ring-down sequences. Homodyne beats will emerge when the resonator output is polarized suitably such that both resonator polarization modes contribute the signal. The strong electric field of the matched mode will amplify the weak and beating non-matched field. We also find that the beat frequency

$$f_B = \frac{c}{L_B n} = \frac{c\Delta n}{\lambda n}, \tag{5.2}$$

is independent of the resonator length, and is directly related to the beat length L_B and thus the degree of birefringence Δn. This result is the basis of our work discussed in Section 6.7 and publication [P4].

We erroneously claimed in publication [P3] that Eq. (5.2) is valid for all Δn. In fact, this is true only when the round-trip difference of the non-matched mode remains smaller than π. This limits the applicability of the measurement scheme for cases where $\Delta n < \lambda/(4\ell)$.*

Within the stated limitation, the scheme benefits the enhancements of sensitivity and accuracy. It employs the long effective interaction length provided by a resonator and the

*The limitation of the phase-shift difference $\Delta\varphi = |4\pi n_1 \ell/\lambda - 4\pi n_2 \ell/\lambda| < \pi$ yields directly in the given relation. The reason for the limitation may be illustrated by drawing the transmission comb of the two polarization modes. When the phase-shift difference is greater than π, say, $2\pi + \phi$, the mode beat frequency indicates the phase-shift difference of ϕ omitting the full period of 2π.

weak signal of ellipticity is amplified by homodyne beating. In addition, the measurement is performed as the reading of time instead of intensity. The proposed method may provide very high measurement sensitivity. For example, an empty cavity with a length of 1 m and mirror reflectivity of 99.99% yields in a time constant of 33 μs. If a ring-down sequence contains three beats during the time-constant time, the beat period is 11 μs and the beat frequency is 90 kHz. At a wavelength of 1.0 μm the birefringence thus becomes $0.3 \cdot 10^{-9}$, which is in the vicinity of the sensitivity required for *direct detection* state-of-the-art vacuum birefringence experiments [66].

6 All-optical clock recovery based on fiber resonators

Publications [P4] and [P5] focus on all-optical signal processing and telecommunications technology. In publication [P4] we propose an all-optical clock recovery scheme capable of multichannel signal processing. The method relies on a birefringent optical resonator, whose transmission spectrum is used to filter carrier and sideband frequencies of return-to-zero (RZ) -modulated data for multiple wavelength channels. In a proof-of-principle experiment we perform an all-optical clock recovery for 21 parallel wavelength channels at two simultaneous data rates. In publication [P5] we investigate the feasibility of using sideband filtered signal, combined with a continuous wave light emitted at the carrier wavelength to perform multichannel clock recovery.

6.1 Introduction to optical clock recovery

Clock recovery (CR) is a fundamental operation performed in all digital communications devices ranging from ordinary mobile phones to high-speed optical receiver cards. In a simplified picture, all digital communications systems consist of three main building blocks: a transmitter, a transmission medium, and a receiver. The transmitter and the receiver are typically separated by a considerable distance, and the receiver has no means to obtain direct information about the transmitter clock. Naturally, this information could be sent on separate communications channel, yet, with penalty on the available bandwidth and the cost of the system. Therefore, the receiver typically recovers the clock directly from the incoming flow of bits. The timing information is required for the decision-making process. For each digital bit, the receiver must make a decision about its state. If the decision is made at incorrect moment of time, the reading process is prone to error (see Fig. 6.1).

In optical telecommunications, as in telecommunications systems in general, the clock has traditionally been recovered with electrical circuitry. For a conventional receiver, which converts the optical signal to electrical one the electronic CR is, and probably remains to be, the most obvious choice. There are, however, locations and devices in the telecommunications infrastructure, where the optical-to-electrical conversion is unnecessary, even undesired, and the preferred choice is to preserve the signal in the optical domain. Such devices are an all-optical signal regenerator, a logical optical gate, or some other all-optical signal processing system [72–75].

Optical CR methods may be divided into two main categories: active pulsating and passive filtering techniques. Active pulsating techniques employ an optoelectronic oscillator loop or a self-pulsating laser, which is locked to the incoming flow of bits. The

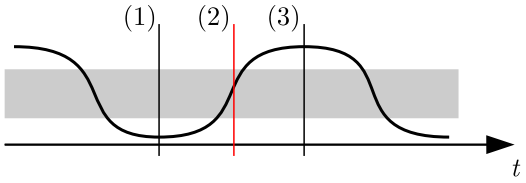

Figure 6.1: Decision-making process for non-return-to-zero modulated data. Correct decision-making times of (1) and (3) provide results of "low" and "high," respectively. An incorrect decision-making moment (2) yields in ambiguous result.

active techniques typically produce a high-quality clock signal, yet, usually with cost of complexity or manufacturing cost. Passive filtering techniques simply remove part of the information from the signal and preserve only the base frequency. The passive filtering techniques typically have simple construction and low manufacturing cost, their challenge being the quality of the recovered clock signal.

6.2 Data modulation and signal spectrum

In telecommunications systems the transmitted information is coded into light by modulating the amplitude, the phase, the frequency, or the polarization of the carrier wave. Two conventional amplitude shift keying schemes, namely the RZ and the non-return-to-zero (NRZ) formats are shortly reviewed.

In RZ and NRZ formats the signal has two possible states: "high" and "low." In the RZ format the bit pulse duration is shorter than the unit interval (total duration of the bit) and in the NRZ format these two durations are the same. In other words in RZ format the signal returns to "low" state between two consecutive "high" state bits, and in NRZ format the signal remains in "high" state. The frequency spectrum of the RZ modulated signal contains the timing information, whereas the NRZ spectrum lacks these features.

A continuous train of RZ modulated pulses (Fig. 6.2a) can be modeled as a convolution

$$s\left(t\right) = \left(\Pi * \text{Ш}\right)\left(t\right), \tag{6.1}$$

of the square pulse (Fig. 6.2b)

$$\Pi\left(t/a\right) = \begin{cases} 1, & |t/a| \leq 1/2 \\ 0, & |t/a| > 1/2 \end{cases}, \tag{6.2}$$

and the comb function (Fig. 6.2c)

$$\text{Ш}\left(t;T\right) = \sum_{n=-\infty}^{\infty} \delta\left(t - nT\right), \tag{6.3}$$

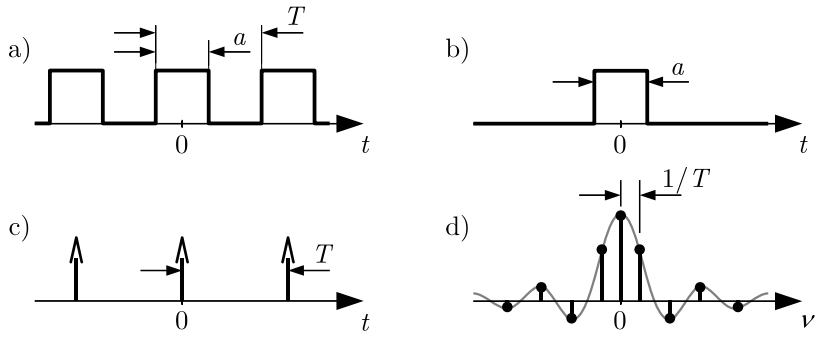

Figure 6.2: Train of pulses may be perceived as (a) a convolution of (b) the square pulse and (c) the comb function. The signal spectrum (d) contains discrete peaks.

where a and T are the pulse duration and the repetition period, respectively. According to the convolution theory the Fourier-transform* of the pulse train can be written as

$$\begin{aligned} S(\nu) &= \mathcal{F}\{\Pi\}\,\mathcal{F}\{\text{Ш}\}(\nu) \\ &= \frac{a}{T}\operatorname{sinc}(a\nu)\sum_{k=-\infty}^{\infty}\delta\left(\nu-\frac{k}{T}\right), \end{aligned} \tag{6.4}$$

which provides the baseband spectrum (Fig. 6.2d) of the signal. After the modulation to a higher (optical) frequency the spectrum is just shifted accordingly, but its shape and magnitude remain intact. Due to repetitive nature of the time-domain signal, the spectrum consists of discrete peaks with an envelope of a sinc-function.† The peaks are separated by the repetition frequency $1/T$ and the sinc-envelope depends on the pulse duration a. When the pulse duration a approaches the repetition period T the time-domain signal does not reach zero between the two upper state bits and the modulation is in NRZ form. As we will discuss in Section 6.6 the clock may not directly be recovered from pure NRZ data, because then the zeros of the sinc-envelope coincide with the spectral peaks and the spectrum lacks the discrete spectral features at frequency separation of $1/T$ (see Fig. 6.3).

Real data obviously consists of a collection of "high" and "low" level bits, not just a train of "high" states, and the signal spectrum follows the shape of pulse spectrum envelope. Even then the peaks of the RZ signal spectrum typically contain more energy than the surroundings. The aim of all clock recovery schemes is to amplify or filter these spectral features such that the original clock frequency may be recovered.

*We use the following definition for the Fourier-transformation

$$X(\nu) = \mathcal{F}\{x\}(\nu) = \int_{-\infty}^{\infty} x(t)\exp(-i2\pi\nu t)\,dt.$$

†The normalized form reads as

$$\operatorname{sinc} x = \frac{\sin \pi x}{\pi x}$$

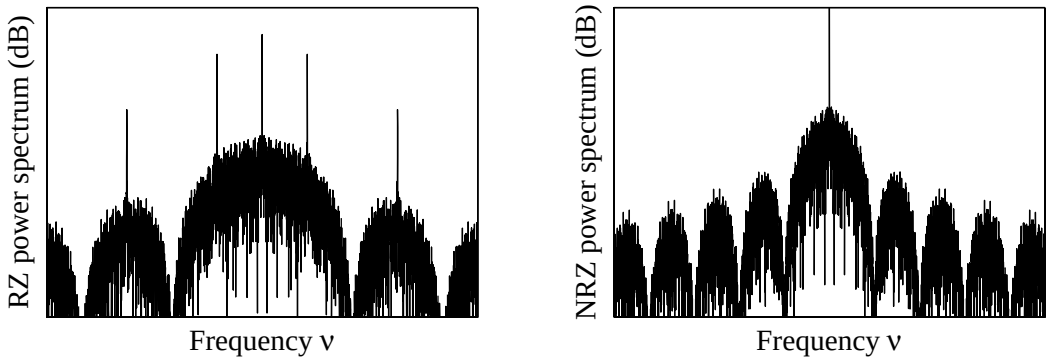

Figure 6.3: The power spectra of simulated pseudo-random RZ (left) and NRZ (right) data.

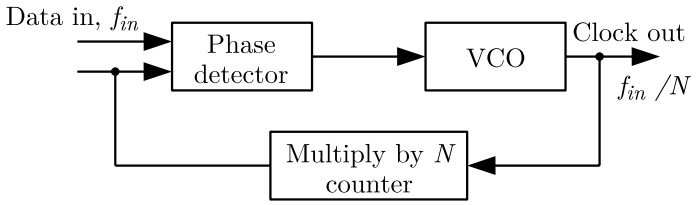

Figure 6.4: Schematic illustration of components of a subharmonic PLL.

6.3 Phase-locked loops

A common self-pulsating technique is to use an optical phase-locked loop (PLL). The function of the optical PLL closely imitates a conventional electrical PLL that is extensively used in applications of radio frequency (RF) and telecommunications technology. The PLL, whether optical or electrical, synchronizes an internal signal oscillator with an external reference signal, which typically is an arriving stream of data. Through the synchronization process the PLL obtains information about the frequency and the phase of the reference signal, which otherwise may be buried under the data modulation. The PLLs are used especially for subharmonic clock recovery, such as recovery of 10-GHz base-clock from 100-Gbit/s optical time-division multiplexed (OTDM) stream.

The conventional electrical PLL is composed of three basic components: a phase detector, a voltage-controlled oscillator (VCO), and a feedback loop. Additionally, the control loop may consist of a multiplication counter, when the resolved oscillation is a subharmonic of the reference signal (see Fig. 6.4). The synchronization is made by adjusting the VCO such that the cross-correlation value of the reference and local signals is maximized.

Modern telecommunications infrastructure operates routinely at data rates of 10 Gbit/s and experimental systems have reached data rates of 160 Gbit/s and beyond. The electrical PLL will ultimately be limited by the phase detector response time [76], and the scientific community has studied alternative optoelectronic techniques to perform the required cross-correlation.

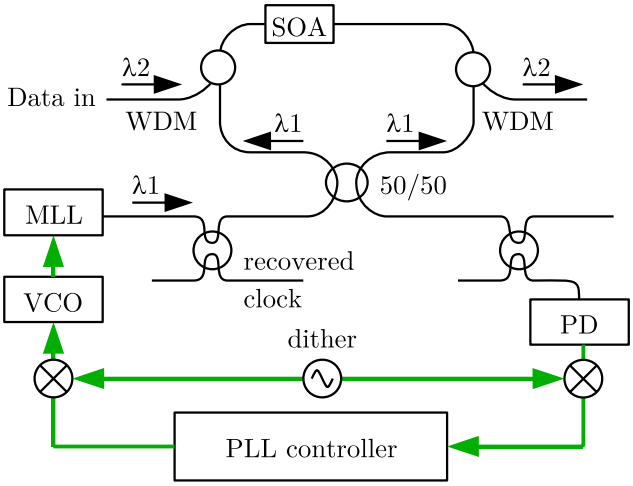

Figure 6.5: Nonlinear optical loop mirror based optical PLL [82]. Symbols: MLL–mode-locked laser, PD–photodiode, WDM–wavelength selective add/drop-multiplexer, thick lines–electrical connections, thin lines–optical connections.

When compared to other optical CR methods, the optical PLL setups often suffer considerable complexity. However, the recovered clock quality in terms of jitter and stability is typically high and PLLs provide the possibility for subharmonic CR, which by other methods may not be attainable.

PLL using optical gatesgree

The first publication using optical, instead of electrical cross-correlation was made in 1988 by S. Kawanishi and M. Saruwatari, who suggested the use of electrical gain modulation in a semiconductor optical amplifier (SOA) [77]. In the proposed scheme the SOA is used as an optical gate, whose state is controlled by RF modulation. The scheme is simple, but due to limited SOA carrier recombination time the data rates remain at 1 Gbit/s and below. The SOA gain modulated PLL was developed further by using optical modulation [78–80], which permits an order of magnitude higher data rates.

Instead of gain modulation, an optical PLL may also be based on amplitude modulated optical gate, which compares the frequency and phase of the local optical clock with the incoming stream of data. The gate mechanism can be based on a nonlinear optical loop mirror (NOLM) [81–84], an electronically gated electroabsorption modulator (EAM) [85–92], an optically gated EAM [93–96], or a $LiNbO_3$ modulator [97–99]. An example of NOLM based optical PLL is depicted in Fig 6.5.

Nonlinear cross-correlation methods

The required cross-correlation of the local optical clock and the data signals can also be performed through four-wave mixing (FWM) in a nonlinear optical medium, such as

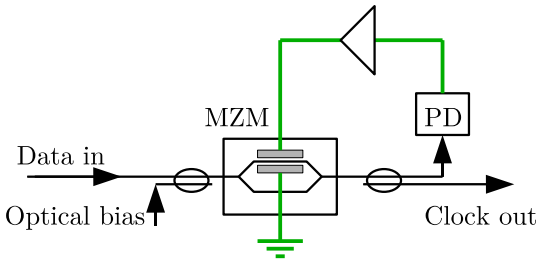

Figure 6.6: Clock recovery with an OEOL incorporating a Mach-Zehnder modulator [11]. Symbols: MZM–Mach-Zehnder modulator.

an SOA. The pulses, depending on the degree of overlap, interact through the FWM process and provide the cross-correlation of the signals. The generated wavelength is bandpass filtered and the information about the time averaged measured optical power is fed back to the VCO [100–104].

Recently, another nonlinear cross-correlation method was introduced that is based on two-photon absorption in silicon avalanche photodiode [105, 106]. The time averaged photodiode response is dependent on the temporal overlap of optical pulses and can thus be incorporated in PLL synchronization.

Oscillating electro-optic loops

The construction of the optical PLLs discussed above follow the basic structure of the conventional electronic device, just the cross-correlation performing phase comparator has been replaced with proper optical or optoelectronical components. Especially, the VCO has characteristically been a discrete microwave source that has either directly modulated an optical gate (see, e.g., Ref. [105]), or it is used to synchronize a pulsed light source, such as a mode-locked laser (MLL; see e.g., Ref. [106]). A number of optical PLLs differ in this respect from the previous treatment. In those, the microwave VCO has been replaced with an oscillating electro-optic loop (OEOL), which combines the functions of the feedback loop and the VCO.

In 1991 M. Chbat *et al.* demonstrated clock recovery in OEOL that consisted of a Mach-Zehnder modulator (MZM) and an amplified feedback loop, which circulated the output back to the control port of the modulator [11] (see Fig. 6.6). In such arrangement the free-running oscillation frequency is obviously dependent on the feedback loop length and the response times of the photodiode and the modulator. In this demonstration the operation frequency remained 13.6 MHz, and the authors suggest higher operation frequencies by monolithic integration of the modulator and the feedback loop components. This demonstration of OEOL makes efficient use of the MZM, which is simultaneously used as the phase comparing cross-correlator and the intensity modulating device.

The dependency of the operation frequency to the feedback loop length may be relaxed when a narrow-band RF filter is added in the loop to filter out all frequencies, except a desired higher harmonic of the base tone. An early demonstration by X. S. Yao and

G. Lutes in 1996 employed an OEOL, where the cross-correlation was performed with a photodiode and the light was modulated with a MZM [107]. A similar setup was used recently by H. Tsuchida and M. Suzuki [108], who successfully performed 40 Gbit/s optical CR. Photodiode based cross-correlation in OEOL has been performed also in conjunction with a MLL oscillator [109].

The optical CR has been demonstrated by use of a bandpass filtered OEOL, which performs the cross-correlation with one or more EAMs and use photodiodes only for opto-electrical conversion [110, 111]. A recent development in EAM based OEOL has been the use of a traveling-wave EAM, whose filtered and amplified photocurrent is fed back to the EAM control port [112–115]. This interesting approach provides the opportunity not only for optical CR, but also optical reshaping function, which together are needed in optical regeneration.

Simultaneous demultiplexing and clock recovery of a 10-Gbit/s signal from a 160-Gbit/s OTDM stream in OEOL was performed with a mode-locked laser as the pulse source and Mach-Zehnder switch as the cross correlator [116].

6.4 Self-pulsating lasers

Optical CR can be performed by injecting an optical input into a self-pulsating laser, whose output is locked to the base-frequency of the input. This method typically yields simple design and a high quality regenerated clock signal. Also, the absence of RF electronics in most proposed self-pulsating laser methods enables operation at frequencies greatly surpassing the optical PLLs. From a practical point of view the adoption of self-pulsating lasers is challenged by the manufacturing cost of devices.

Mode-locked self-pulsating diode lasers

In 1988 M. Jinno and T. Matsumoto introduced a two-section self-pulsating distributed feedback (DFB) diode laser for all-optical CR [12]. The bias current of the two laser sections had opposing sign, i.e., the other section was reverse biased that made it act as a saturable absorber (SA)—an essential component of a MLL. As the name implies, the absorption of the SA is dependent on the intensity of light. When a broadband active medium, whose gain curve spans over several longitudinal modes, is combined with a suitable SA the intracavity oscillation of the modes are coupled and the laser produces a continuous train of short pulses. When the base-frequency of the injected signal is within the locking-range of the MLL the injection-locking may occur and the MLL may be used for optical CR.

The operation in the seminal work was demonstrated for a moderate data rate of 200 Mbit/s that was limited by the carrier lifetime of the SA region. When this region is doped with suitable dopant, such as Zn or N, and the SA region is suitably biased the carrier lifetime could be reduced and the operation was demonstrated for

data rates of 5 Gbit/s [117–120], and 10 Gbit/s [121, 122], respectively. The impact of SA biasing conditions for MLL performance has been studied in Ref. [123].

In passively mode-locked lasers the cavity length determines the free-running pulse repetition frequency. The MLL using semiconductor technology benefits the possibility of short cavities, which results in high repetition rate. A mode-locked semiconductor laser has been demonstrated for optical CR of 160-Gbit/s stream [124].

Regeneratively mode-locked semiconductor diode lasers have shown a promise for subharmonic clock recovery. Under injection of OTDM signal the MLL have been shown to produce a weak subharmonic frequency, which may be amplified in a feedback loop.* The operation has been demonstrated for recovery of 40 GHz [125, 126], 80 GHz [127], and 160 GHz [128], clock from 160-Gbit/s OTDM stream. Subharmonic CR has been demonstrated also in Refs. [122, 129, 130].

Other self-pulsating multisection diode lasers

The self-pulsation in a laser diode does not necessarily require an SA. It may also be achieved by use of a multisection laser diode with unequal section lengths. Clock recovery in a two-section DFB laser was demonstrated up to 20 GHz in early experiments [131–133]. This type of a self-pulsating laser has sinusoidal output (unlike MLL), which typically is undesirable for OTDM demultiplexing, but sufficient for other types of synchronization. The pulsation frequency may be tuned by adjusting the current of the two sections, which affects the carrier density of each section.

The two-section DFB laser based CR has two possible modes of operation, coherent and incoherent one. In the incoherent scheme the carrier density is modulated when the signal is injected at approximately 1 nm away from the free-running wavelength. The required injection power is sufficiently high (about 0 dBm), but the operation is polarization and wavelength independent. In coherent operation the injection occurs at the free-running wavelength. Then only weak (about -13 dBm) optical injection is required, but then the method is dependent on the state of polarization and the wavelength of injection. Wavelength and polarization independence may be achieved when an SOA based wavelength conversion is used prior to the CR DFB laser [134–137]. The coherent diode laser based CR operation has been demonstrated up to 100 Gbit/s. The theory and operational dynamics of coherent and incoherent diode laser based CR is discussed in detail in Refs. [138, 139], and summarized in Table 6.1.

The performance of the two-section self-pulsating laser may be improved by adding a phase tuning section between the two existing sections. The first section of the three-section device provides amplification (lasing), whose current determines the self-pulsation frequency. The second section tunes the phase and thus optimizes the self-pulsation. The third section provides feedback through the DFB structure. This section is typically driven at the transparency current and it acts as a reflector at the lasing wavelength. Operation speed of the three-section device have been demonstrated up to 40 GHz [140–

*This scheme could be classified under the umbrella of optical PLL methods.

Table 6.1: Characteristics of coherent and incoherent self-pulsating multisection diode laser based CR [134, 138, 139].

	coherent CR	incoherent CR
CR method	injection locking	carrier modulation
carrier density	stable	modulated
achievable CR rate	virtually unlimited	limited by carrier dynamics
injection power	low (−13 dBm)	high (0 dBm)
bit-pattern sensitivity	insensitive	sensitive
polarization sensitivity	sensitive	insensitive
wavelength sensitivity	sensitive	insensitive
injection wavelength	at free-running wavelength	typically 1 nm away

145]. In on-going development the multisection laser diodes have incorporated four [146], and five [147, 148] separate sections.

In a separate development also FP type diode lasers have been suggested for use in all-optical CR. The length of a multimode FP laser cavity determines the set of possible oscillation frequencies. In the free-running state the mode competition causes continuous fluctuation and instability in laser output, but under suitable optical injection only the desired modes are amplified and the laser provides the data clock [149]. This method relates to a passive FP based CR method we will discuss in more detail in Section 6.5. The jitter characteristics of a self-pulsating quantum dot FP semiconductor laser was recently investigated in Ref. [150].

Self-pulsating mode-locked lasers with fiber loop feedback

The possibility to use fiber based laser for all-optical CR was explored already in 1992 by K. Smith and J. K. Lucek [151]. They constructed a mode-locked fiber loop, which shared a length of fiber with the data transmission line. The mode locking occurred through the process of cross-phase modulation in the shared fiber section. The CR was demonstrated for data rate of 1 Gbit/s [151], and in a subsequent work for 40 Gbit/s [152]. In succeeding development the long section of the shared fiber was replaced with a NOLM [153], and an SOA [154–156]. The same principle was also used for CR of multiple simultaneous wavelength channels by utilizing an SOA array module [20]. In this configuration the fiber loop circulation and the injected data co-propagate in the same direction and the laser gain is provided by an erbium-doped fiber amplifier (EDFA).

In 2000 Vlachos *et al.* introduced a MLL loop with counter-propagating clock and data signals, where a single SOA simultaneously provided the amplification and the mode-locking through the gain modulation [157] (see Fig. 6.7). This simple, yet, efficient scheme has been studied further and demonstrated for subharmonic [158], and wavelength-switchable CR [159].

A particular challenge of the SOA based mode-locking is the pattern effect, which means that the recovered clock pulses fluctuate according to the input data pattern. The reason

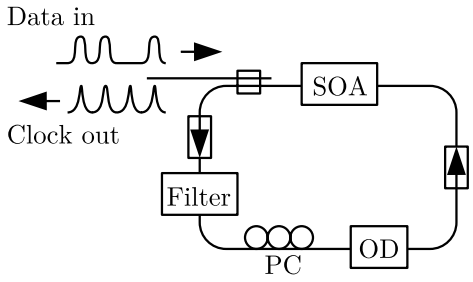

Figure 6.7: Mode-locked fiber laser with a single SOA, which provides both the amplification and the mode-locking through the gain modulation [157]. Symbols: PC–polarization controller, OD–optical delay.

for this fluctuation is the SOA carrier density recovery time, which is several hundreds of picoseconds [160]. The pattern effect has been compensated by applying a CW beam injection [154, 161], an additional SOA at the laser output [157], preprocessing by a FP resonator [160], or a FP resonator combined with an additional SOA [162].

Subharmonic CR at 10 GHz from 160-GHz OTDM stream has been achieved with a fiber loop MLL [163]. Instead of the conventional SOA the required nonlinearity was achieved with a linear optical amplifier and the loop amplification was provided by a separate EDFA. The linear optical amplifier consists of an amplifying semiconductor waveguide combined with a vertical-cavity surface-emitting laser such that the amplifier and the laser share the active region. The linear optical amplifier provides improved mode-locking, because it produces no phase shifts for small input signals.

In 2000 Y. Su *et al.* proposed a parametrically amplified fiber loop for all-optical CR [164]. The FWM process occurred in a dispersion shifted fiber and the incoming data stream was used as the pump signal. The process was seeded by amplified spontaneous emission noise of the EDFA and the idler and the pump signals were suppressed with a tunable filter. The clock pulse amplitudes were equalized through gain-saturation of the FWM process. The amplification of the EDFA was kept slightly below the round-trip loss of the loop, such that the lasing process was generated through the parametric process, not due to EDFA amplification. The scheme has been proposed for multiwavelength CR by Kuksenkov *et al.*, who recently demonstrated a variation of the scheme for two simultaneous wavelength channels [19].

Fiber MLL based CR have been realized also by two-ring MLL [165], figure-8 configuration [166,167], linear fiber cavity with a Faraday rotation mirror and an NOLM [168–170], amplified fiber loop that consists of an SOA and grating filter based wavelength converter [171,172], and a fiber loop that incorporates a multiple-quantum-well semiconductor SA [173]. In these demonstrations the injection locking occurs through an OEOL, SOA phase modulation, a cross-phase modulation in a dispersion-shifted fiber, SOA gain modulation, and loss-modulation in the SA, respectively.

6.5 Filtering methods

Clock recovery does necessarily not require a self-pulsating arrangement. It can also be performed by filtering methods, which only select the desired spectral features of the input signal (see discussion about signal spectra in Section 6.2 above).

Fabry-Pérot filters

As shown in Section 2.1 the transmission spectrum of a FP resonator is periodic and the transmission band is typically narrow. This makes the FP resonator an effective filter, whenever the filter periodicity is allowed, or even desired. In 1990 M. Jinno *et al.* constructed a CR arrangement with a free-space FP resonator [13], whose FSR matched with the data rate and thus the clock tone separation frequency of the RZ modulated input signal. When the clock tones of the signal coincided with the resonator transmission bands, the clock of the signal was recovered. The scheme has been demonstrated also for a fiber-loop resonator [174]. While the scheme is fully passive and uses no nonlinear components (such as an SOA), the operation speed of the method is virtually unlimited (depending on resonator length) and the CR operation may be extended to several simultaneous wavelength channels [17].

The challenge of the FP filter based CR is the pattern effect, i.e., depending on resonator time constant and the input pattern of the data stream, the output of the filter may fluctuate considerably (see, e.g., Fig. 3 in publication [P4]). The resonator output equalization has been made with a number of schemes, such as ultra-fast nonlinear interferometer [175–179], where the clock signal with fluctuating amplitude controls the phase response of an SOA, which is saturated by CW light. Due to SOA nonlinear response the counter-propagating CW beam experiences a phase shift of π such that its polarization delayed components interfere at the output of the interferometer. This equalization scheme has been demonstrated up to 40-Gbit/s data rate with co-propagating the CW and the fluctuating clock beams [14]. The filtered clock signal equalization has been demonstrated also with Mach-Zehnder interferometric switch [180].

In order to recover the clock for as many consecutive low-level bits as possible and to minimize the pattern effect, a resonator with the longest possible time constant is preferred. The photon lifetime is inversely proportional to the bandwidth as indicated in Eq. (2.6). Thus, a long time constant inevitably results in a narrow transmission band. Because the carrier wavelength of the transmitter always has a tolerance, the time constant and the number of recovered low-level bits are limited. For example, to resolve 10 consecutive low-level bits within the $1/e$ period at the data rate of 100 Gbit/s results in a linewidth requirement of ca. 1 GHz (see Fig. 6.8).

A very simple, yet, efficient amplitude equalization scheme has been demonstrated by combining the FP resonator output with an SOA that is operated close to the gain saturation region. The optical clock pulses with low amplitude are amplified normally, and the clock pulses with high amplitude are limited due to gain saturation of the SOA. This simple scheme has been demonstrated for data rates of 10 and 40 Gbit/s [181,182],

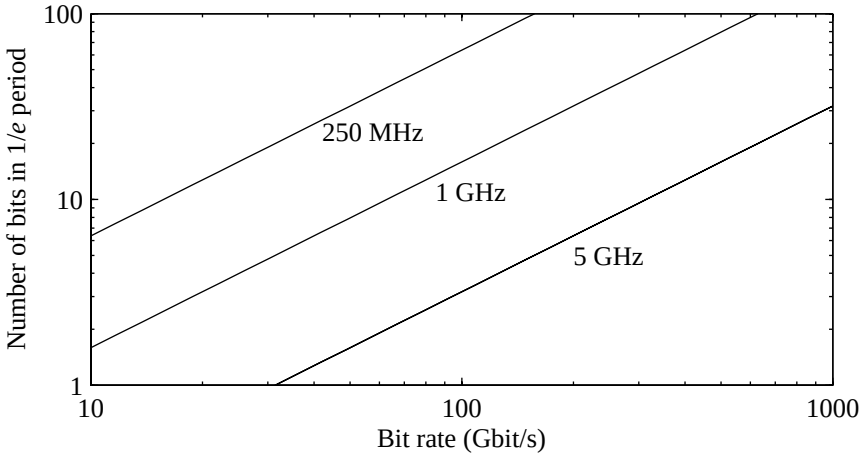

Figure 6.8: Number of resolved bits for varying data rates and resonator bandwidths.

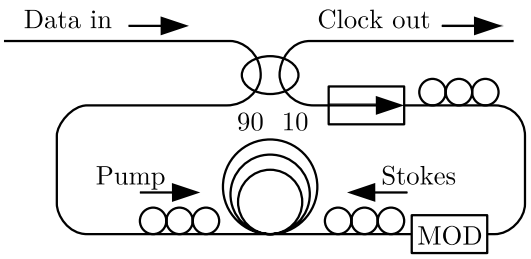

Figure 6.9: Stimulated Brillouin scattering CR setup [15].

respectively. Some recent demonstrations of all-optical regeneration have utilized this particular CR method [183, 184].

Stimulated Brillouin scattering filters

A novel CR scheme developed by D. L. Butler *et al.* in 1995 uses stimulated Brillouin scattering effect for active filtering of the clock tones of the data spectrum [15] (see Fig. 6.9). The incident data stream is divided into two counter-propagating arms (90/10). The stronger arm is used as the pump wave, and the weaker arm as the seed wave, which is downshifted by 10.9 GHz to the Stokes frequency. When the pump and Stokes waves convolute each other, only the strongest spectral components are amplified and the clock is recovered. The scheme benefits of wavelength and data rate transparency unlike most other CR schemes. The scheme has been demonstrated for multiwavelength system, where the processing was made for two simultaneous channels at data rate of 10 Gbit/s [18]. The stimulated Brillouin scattering CR setup performance is theoretically investigated in Ref. [185].

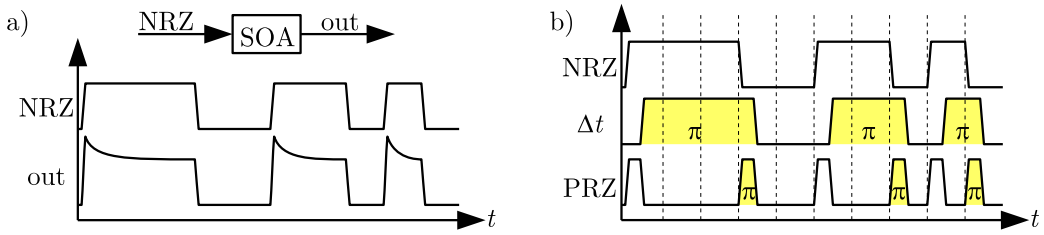

Figure 6.10: Clock component generation into NRZ modulated data: (a) SOA generated overshoots at leading pulse edges, and (b) subtraction of delayed data results in pseudo-RZ modulation, which can be used to direct some nonlinear component, such as optical gate (modified after Ref. [170]).

Bragg grating filters

Filtering of clock tones of the data spectrum can be achieved also with fiber Bragg gratings, which are tuned to carrier and sideband frequencies. When a pair of such filters are combined with a circulator and a variable optical attenuator, the clock has been recovered for 40-Gbit/s NRZ signal [16, 186]. The ability to recover the clock of a NRZ modulated signal refers to the high data rate, where the finite rise and fall time of the pulses create clock tones. The CR for NRZ modulated signals is elaborated in the following Section 6.6.

6.6 Clock recovery of NRZ modulated data

As noted in Section 6.2 the pure NRZ modulated signal spectrum lacks the discrete clock tones, which are required for injection locking or filtering. Therefore, the CR may not be performed directly for the pure NRZ modulated data, but the missing clock frequency components must be modulated onto the signal before the CR operation.

A common method is to use self-phase modulation of an amplified semiconductor device, such as an SOA [119, 120], or a diode laser [187], which generates an overshoot at each leading data edge due to gain saturation (see Fig. 6.10a). This overshoot contains the needed clock component. In order to enhance the suppression ratio between the clock component and the NRZ modulation component, the SOA is often accompanied with an optical filter, such as a bandpass filter [169, 188], a circulator accompanied fiber Bragg grating [189–191], or a periodical WDM demultiplexer [192, 193]. The cross-gain modulation of an SOA has also been used for clock tone generation, where the SOA has been a part of the fiber MLL ring [194–196].

Another clock tone generation scheme is to convert the NRZ modulation to RZ or pseudo-RZ modulation. This is done by dividing the NRZ signal in two parts, which are delayed with respect to each other—the delay being typically less than one bit period. When the electric fields interfere destructively with each other, a RZ resembling signal is generated

(see Fig. 6.10b). However, this signal *does not* contain clock components yet.* When this signal is directed to a nonlinear element, such as a NOLM gate [168,170], or a photodiode [197], the clock tones appear. A variation of the scheme has been demonstrated also by four-wave mixing process [198].

Recently, direct CR of 40-Gbit/s NRZ modulated data has been demonstrated without nonlinear preprocessing. This has been possible, because the optical spectrum of 40-Gbit/s stream typically contains weak clock components due to limited rise and fall time of the NRZ signal [199]. The challenge of CR is to use these weak clock tones. The clock component enhancement has been achieved with a FP filter [200], and fiber Bragg gratings [16, 186, 199].

6.7 Multiwavelength all-optical clock recovery using birefringent FP resonator

In publication [P4], we propose a new passive all-optical CR scheme that is based on a simple device consisting of a birefringent resonator and a polarizer. The scheme offers the possibility for parallel processing of several simultaneous wavelength channels and data rates. The feasibility of the scheme is demonstrated for 21 simultaneous wavelength channels, one channel hosting a data rate of 40 Gbit/s and the remaining channels a data rate of 10 Gbit/s. To the best of our knowledge, this is the first demonstration of parallel optical signal processing at different simultaneous data rates. All-optical CR has earlier been reported for two [18,19], and four [20], simultaneous wavelength channels. In terms of channel count our results demonstrate an improvement of 5-10 times compared to the current state-of-the-art.

The experimental setup of publication [P4] was built in spirit of publication [P3], where the mode beats were generated for rising and falling edges of data pulses. Although the basic operation principle is the same, the publications bear a difference in the way the theory is presented. In publication [P3] the observed phenomena are explained using time-domain phasor formalism, whereas publication [P4] uses frequency-domain analysis.

Operating principle

As discussed earlier in this Chapter, the CR methods are divided into two main categories: the self-pulsating and the filtering methods. Our scheme belongs to the group of classical filtering methods, relying on transmission properties of a passive FP resonator and it closely resembles the conventional FP filtering methods [13, 174, 182], with a notable exception: in contrast to all earlier works we used a birefringent resonator. As explained in publication [P4] a birefringent resonator may be perceived as a pair of orthogonal resonators with virtually equal FSR, but detuned transmission spectra. When the frequency difference of the transmission maxima, which may be tuned by the degree

*The reason: a set of linear operations, such as the time shift and the summation do not create the clock tones.

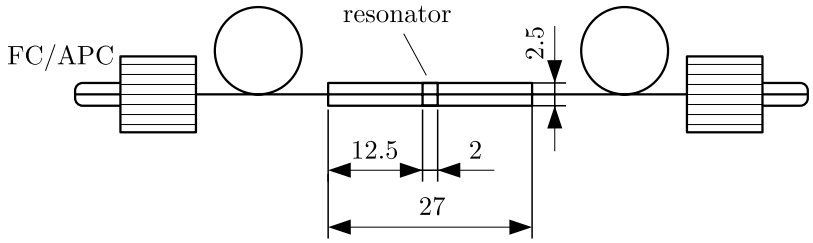

Figure 6.11: Construction of the pigtailed resonator. Drawing not in scale. Units: mm.

of birefringence, equals to the data rate frequency, say 10 GHz, CR may be performed for multiple simultaneous wavelength channels. Of course, this could have been done already with conventional FP resonators, but then both the channel grid and the data rate frequencies are bound to integer multiples of the FSR. Using the birefringent resonator, the data rate may be matched with the degree of birefringence and the channel grid with the FSR.

The resonator and the clamp

The experimental setup of the clock recovery work has been discussed in publication [P4]. In the following, we review and provide background information about the construction and characteristics of the two most important components, namely the birefringent resonator and the clamp.

The construction of the pigtailed resonator is shown in Fig. 6.11. The resonator medium is a 2-mm-long piece of single-mode fiber with highly reflective coatings on the end-facets, concealed in a glass ferrule (FSR = 49.9 GHz, FWHM bandwidth of 645 MHz). The resonator bandwidth is obtained from the photon lifetime $\tau = 247$ ps (at 1550 nm), which was measured with a series of cavity ring-down measurements. The photon lifetime of the resonator is an important factor, which determines the number of digital zero-bits for which the clock signal can be recovered. For 10- and 40-Gbit/s signals the measured lifetime predicts approximately 3 and 12 recovered zeros, respectively.

In our experiment the lowest filtered data rate is 10 Gbit/s. According to Eq. (10) of publication [P3] the beat frequency f_B of 10 GHz is obtained when the birefringence

$$\Delta n = \frac{n\lambda f_B}{c} = 7.6 \cdot 10^{-5}. \tag{6.5}$$

Pure and stress-free fused silica is an isotropic medium. The required birefringence may be created in fused silica through geometrical deformation, e.g., stress or bent. In our case the required stress

$$\sigma = \Delta n / C = 22 \text{ N/mm}^2, \tag{6.6}$$

where the stress optical coefficient of fused silica $C = 3.4 \cdot 10^{-12}$ Pa^{-1}. The literature value of the fused silica compressive strength of 1250 N/mm^2 [201] is almost two orders of magnitude greater than the required stress. This suggests that the resonator should be

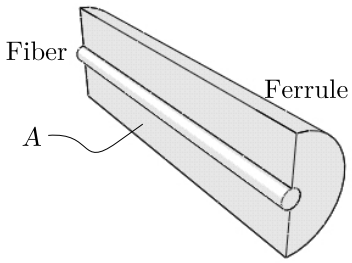

Figure 6.12: A cross-sectional view of the ferruled fiber resonator, where A denotes the cross-sectional area perpendicular to the applied force.

able to sustain the induced geometrical deformation, provided that the stress is applied homogeneously along the ferrule.

Using the geometries of Figs. 6.11 and 6.12 we obtain the ferrule cross-sectional area $A = 27\ \text{mm} \times 2.5\ \text{mm} = 76.5\ \text{mm}^2$. On the presumption that the ferrule and the ferruled optical fiber resonator possess the same value of elasticity, the estimate of the required force F for the desired birefringence is $F = \sigma A = 1683$ N.

In our experiment the stress is induced by a clamp presented in Fig. 6.13. The jaws of the clamp move along the rails and press the ferruled resonator. The force is applied by a screw, which presses a pack of jaws and a silicon spring against a force cell. The rails control the position of the jaws and the direction of the force. The jaws and the rails were machined with tight tolerances in order to ensure precise positioning of the inner grooves of the jaws (see Fig. 6.13c) and the ferrule. The magnified view of the inner groove is illustrated in Fig. 6.13d, which shows that the groove radius of curvature is intentionally 500 μm larger than the radius of the ferrule in order to allow minor ferrule deformation. The groove was spark eroded, which is estimated to provide less than 5 μm average surface roughness. A smooth contact surface is imperative for the setup, because the ferrule and the fused silica resonator are potentially exposed to pressing forces of over 1000 N. Although the compression strength of both materials are beyond the applied stress, even a small kink on the groove will undoubtedly shatter the ceramic material. Therefore, the jaws were additionally coated with 50-μm thickness of polytetrafluoroethylene (PTFE), also known by brand name Teflon®. The PTFE is a soft polymer and the coating creates an elastic buffer between the hard ceramic ferrule and the metallic jaw. Also, the PTFE is known for its low-friction properties. Friction-induced stress between the hard materials could potentially damage the ferrule. These precautions proved successful. At the time of this writing the setup has been working one-and-half years under unceasing pressing force of about 1000 N. Since the initial deployment of the setup the transmission has dropped about 10 dB, which is believed to occur due to damaged fiber pigtails. The resonator itself is assumed to be intact, because the time constant has remained unchanged.

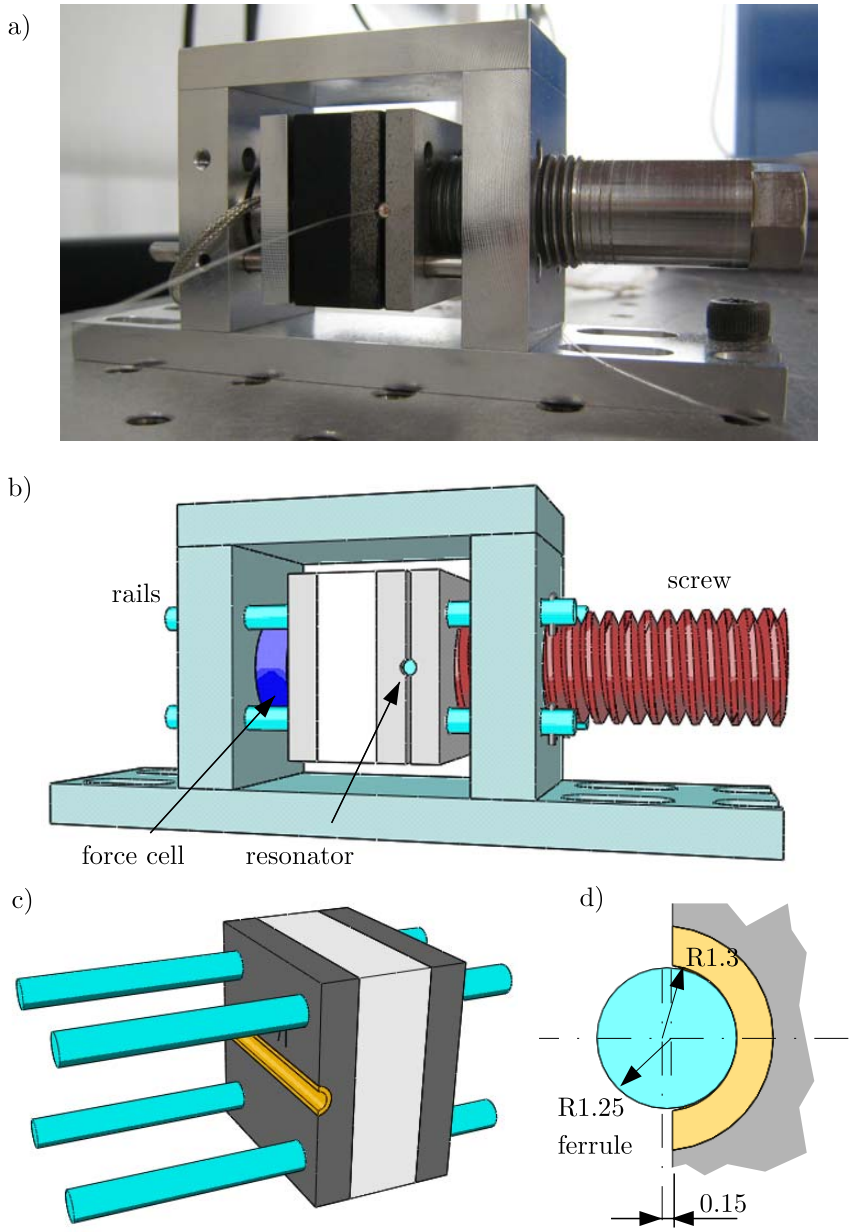

Figure 6.13: The clamp: (a) a photo, (b) a CAD rendered view, (c) a jaw, and (d) a magnified detail of the groove. CAD drawings not in scale. Units: mm.

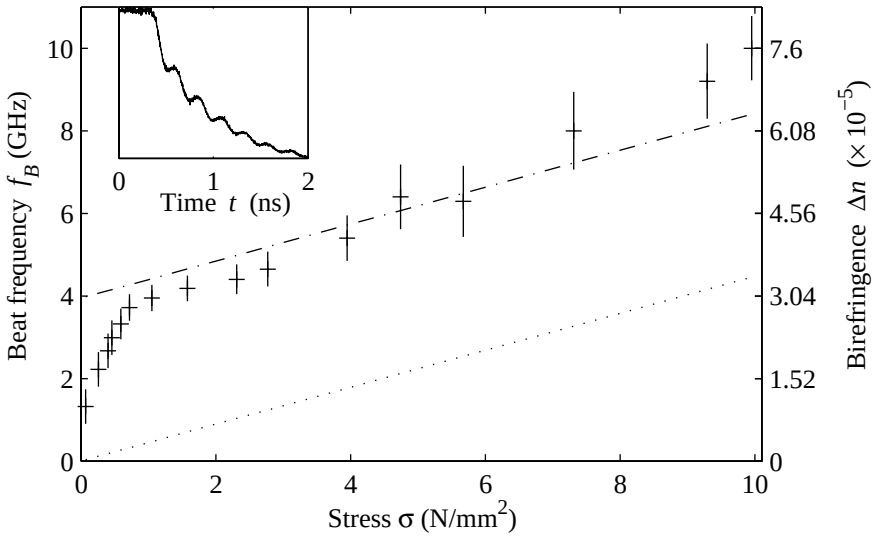

Figure 6.14: Measured beat frequencies f_B for applied stress σ. Right hand axis shows the calculated birefringence Δn. The dotted line represents the theoretical prediction of the birefringence for fused silica stress-optical coefficient $C = 3.4 \cdot 10^{-12}$ 1/Pa, and the dash-dotted line shows the same curve with some offset. Inset at upper-left corner exemplifies a beating ring-down signal for stress $\sigma = 1.58$ N/mm^2.

Characteristics of the birefringent resonator

In our experimental setup, the birefringence was applied by gradually increasing the pressing force of the clamp while recording the beating ring-down signals. The resolved beat frequencies f_B are plotted in Fig. 6.14 for applied stress σ. The calculated birefringence scale is shown on the right-hand side of the graph. For comparison, theoretical fused silica stress-birefringence-relation is depicted with dotted line and the relation with some offset with dash-dotted line. The slope of the theoretical line follows closely the measured data, except in low-stress region. We assume that the deviation is a consequence of two factors. First, the intact (stress-free) resonator exhibits some initial birefringence, probably due to residual stress at dielectric mirrors and in resonator medium. Secondly, the glued sections of the ferrule are aligned (on micro-meter scale) along the grooves when the stress is applied. This induces additional parasitic birefringence on mirrors. Once the setup is settled the change in the measured birefringence is only due to stress-optical phenomenon and the data thus follows the predicted slope.

As discussed, the birefringence creates two independent resonance modes for orthogonal states of polarization. This is manifested as a separation of the transmission maxima of the comb spectra. We verified the findings of Fig. 6.14 and fine tuned the stress by using broadband light source and an optical spectrum analyzer (OSA). The stress of the clamp was carefully changed till the separation of the transmission maxima reached 10 GHz, as depicted in Fig. 6.15. The figure also shows two calculated spectra for a resonator with a FSR of 49.9 GHz, a separation of 10 GHz, and a bandwidth of 645 MHz. Note that the resolution of the OSA (0.06 nm) prevented the observation of the sharp spectral

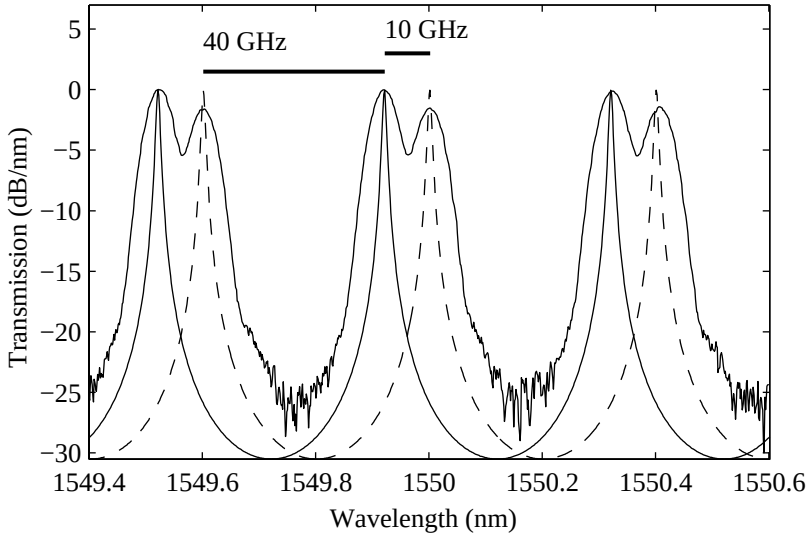

Figure 6.15: Normalized transmission spectrum of the birefringent resonator. Underneath the measured spectrum are two calculated resonator spectra with FSR of 49.9 GHz, separation frequency of 10 GHz, and bandwidth of 645 MHz. Separations of 10 and 40 GHz are marked.

features. As evident from the figure, one can simultaneously filter 10- and 40-GHz frequencies while maintaining the FSR of 50 GHz.

6.8 Clock recovery based on heterodyne beats of sideband-filtered signal

In publication [P5], we investigate the feasibility to use sideband filtering of RZ modulated signal for all-optical clock recovery. The clock beat may be recovered, when the sideband filtered signal is combined with CW light emitted at the carrier wavelength. The benefit of the arrangement is that the number of recovered zeros (due to pattern effect) may be doubled compared to conventional FP resonator based optical clock recovery. We demonstrated the filtering for 23 simultaneous channels at 100-GHz grid, each hosting a data rate of 10 Gbit/s. The investigated method provides the opportunity for multichannel processing, but requires phase matching between the sideband and carrier frequencies.

The challenge of FP resonator based CR is the pattern effect, which affects the quality of the recovered clock. The pattern effect may be reduced when the time constant of the resonator is long enough, yet, with penalty of narrow transmission bandwidth. In real-life systems the emission wavelengths of the transmitter lasers are hardly ever fully stable, which prohibits the possibility to use infinitesimally narrow filter. Therefore, the selection of FP resonator transmission bandwidth is a compromise between opposing demands of robustness of emission wavelength variation and the desire to recover possibly many digital zeros.

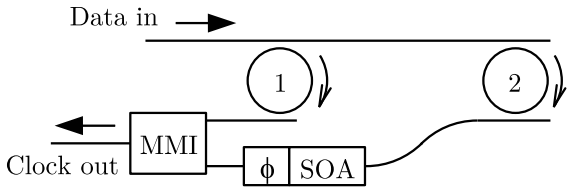

Figure 6.16: A possible CR arrangement. The carrier and sideband are filtered with the ring resonators 1 and 2. Other signal is equalized with a SOA operating close to saturation. The phase is tuned with a phase control section or mechanism. The signals are combined with a multimode interference (MMI) coupler.

The CR process may be perceived as a form of heterodyne detection, where two oscillating electromagnetic fields, the carrier and the sideband are filtered from data stream. While both fields exhibit the same pattern effect, the beating obviously bears the same fluctuation in its amplitude. Should other of the filtered signals be constant, the form of the beating signal would be different. Especially, we show in publication [P5] that the time constant of the beat is twice the time constant of the resonator. This gives an opportunity to achieve twice as many zeros recovered than in conventional FP resonator based CR setup, or alternatively the possibility to relax the transmission bandwidth.

This scheme has two particular challenges. The easier one is the need to track the carrier wavelength with the local oscillator. This can be done, e.g., by seeding the local oscillator with the carrier wavelength. The second, and possibly harder challenge is to match the phase of the local oscillator source with the carrier wavelength of the incoming data. We shall assume that the carrier and the sideband electric fields may be presented as $E_i \exp\left[2\pi\nu_i t + \phi_i\left(t\right)\right]$, $i = \{1, 2\}$, respectively. Should the phase term $\phi_i\left(t\right)$ be the same for both fields, then the phase of the beat remains constant (as it should be) and the clock may be recovered. If the phase term $\phi_i\left(t\right)$ varies, and especially, if it varies randomly, the clock may not be recovered.

To solve the challenges of the stable local oscillator and tracking of the carrier phase, we propose the following CR arrangement (see Fig. 6.16). The carrier and the sideband signals are filtered with ring-resonators (1) and (2). One of the signals (chosen local oscillator) is amplified with an equalizing SOA (or equivalent) and its phase is tuned. The local and signal oscillator signals are combined in a multimode interference (MMI) coupler. While the components are integrated on a single substrate, such as InP, the relative phases of the filtered signals may remain constant.

7 Summary and outlook

This dissertation explores new applications of measurement and telecommunications technology based on fiber optical resonators. First the properties of optical resonators were briefly discussed. It was shown that the optical resonator can temporarily store light at a set of frequencies and effectively prolong the optical path length inside the resonator. The enhancement of the effective optical path length is related to the resonator time constant and the transmission bandwidth. This enhancement, and thus the time constant are strongly dependent on the intracavity losses and increase of loss may thus be measured with high sensitivity from the time constant.

In publication [P1] we discussed of the CRD principle and its applications for fiber optical resonators. To the best of our knowledge, we were first to suggest and demonstrate that the fiber CRD method can be extended beyond the measurement of chemical absorption to other physical parameters, such as bending and fiber degradation. We also showed preliminary results of evanescent field absorption measurement.

An attempt was made to measure magnetic field through Faraday rotation, but this measurement proved unsuccessful due to non-impulse type of optical input. During this experiment we observed a beating signal, whose origin, properties, and possible use are elaborated in publication [P3]. We introduced a new sensitive measurement scheme of optical birefringence that was applied for measurement of the beat length of a short section of conventional single-mode fiber, such that the beat length was about 40 times longer than the measured fiber section.

In publication [P2] a computational algorithm for the extraction of the time constant was proposed. We showed that the developed method may yield in meaningful results under excessive noise condition, where conventional and proven time constant extraction algorithms fail.

The second part of the dissertation is devoted to applications of the telecommunications technology. A comprehensive literature study of optical CR technologies and methods was provided. In publication [P4] a FP resonator based filtering scheme that is capable of parallel processing of multiple channels and data rates was presented. In the proof-of-principle experiment the method was demonstrated for 21 simultaneous wavelength channels. In terms of channel count this is about 5-times improvement to the current state-of-the-art. One of the processed channels had different data rate than all others. In this respect our demonstration is first of its kind. In publication [P5] a multiwavelength CR method based on heterodyne beating of the sideband filtered and the local oscillator signals was investigated. The arrangement benefits of prolonged time constant (or alternatively relaxed transmission bandwidth of the FP resonator), but is challenged by the demand of local oscillator coherence properties.

The progress in the fields of measurement and telecommunications technology has not and will not cease in any foreseeable future. Although both fields *per se* are mature, emerging applications will fuel the need for future innovations. The recent advances in micro and nanotechnology will prompt a need of a new highly sensitive and local measurement principles, such as cavity ring-down or cavity enhanced schemes in nanometer scale optical cavities. For example, one may envision a subwavelength scale annular ring, whose evanescent field output selectively probes a highly localized spatial volume.

The progress of telecommunications technology has traditionally benefitted the ever increasing need of available bandwidth. This demand can not be satisfied unless the cost/bit is reduced by a set of new technologies, such as photonic signal processing and advanced electronics packaging. All-optical regeneration alongside with advanced signal modulation schemes will probably be one of the enabling technologies. Photonic integration, and especially silicon photonics are still in early stages of development, but given the general maturity of Si-based fabrication processes, many large corporations, such as Intel have allocated substantial resources for this work. Also the operating speed of semiconductor based components, which traditionally has been rather limited, will increase by use of quantum dot and quantum wire technologies. Maybe the most powerful promise of photonics is the prospect of multiwavelength processing. In this dissertation we have shown it in linear optical medium, but in future the demonstrations in nonlinear media, such as in photonic crystal fibers are likely to become more commonplace.

List of acronyms and symbols

CR	clock recovery
CRD	cavity ring-down
CW	continuous wave
DFB	distributed feedback
EAM	electroabsorption modulator
EDFA	Erbium-doped fiber amplifier
FP	Fabry-Pérot
FBG	fiber Bragg grating
FSR	free spectral range
FWHM	full-width at half-maximum
FWM	four-wave mixing
MLL	mode-locked laser
MZM	Mach-Zehnder modulator
MMI	multimode interference
NOLM	nonlinear optical loop mirror
NRZ	non-return-to-zero
OEOL	oscillating electro-optic loop
OSA	optical spectrum analyzer
OTDM	optical time-division multiplexing
PD	photodiode
PLL	phase-locked loop
PTFE	polytetrafluoroethylene
RF	radio frequency
RZ	return-to-zero
SA	saturable absorber
SOA	semiconductor optical amplifier
VCO	voltage-controlled oscillator
WLS	weighted least square

a	duration of pulse
c	speed of light in vacuum
d	diameter of the fiber core
ℓ	resonator length
n	index of refraction
r	radial distance from fiber center
s	pulse train function
t	time
t_{rt}	resonator round-trip time

A	area
E	electric field
$\mathcal{F}$	Fourier-transform operator
I	intensity of light
L	fractional one-pass intensity loss
L_B	beat length
R	reflectivity (intensity)
T	one-pass transmission (intensity) or duration of bit
δ	impulse function
$\delta\nu$	resonator bandwidth (FWHM)
λ	wavelength of light in vacuum
ν	frequency of light
σ	stress
τ	time constant, or photon lifetime of a resonator
φ	resonator round-trip phase shift
ω	angular frequency, $\omega = 2\pi\nu$
Δ	relative refractive index difference, $\Delta = \frac{n_1 - n_2}{n_1}$
ΔL	change of fractional one-pass intensity loss
Δn	difference of refractive indices, i.e., birefringence
$\Delta\nu$	free spectral range of a resonator
$\Delta\omega$	angular frequency difference
Π	rectangle function (square pulse)
Ш	comb function

Bibliography

[1] C. Vallance, "Innovations in cavity ringdown spectroscopy," New J. Chem. **29**, 867–874 (2005).

[2] R. Engeln, K. G. Y. Letourneur, M. G. H. Boogaarts, M. C. M. van de Sanden, and D. C. Schram, "Detection of CH in an expanding argon/acetylene plasma using cavity ring down absorption spectroscopy," Chem. Phys. Lett. **310**, 405–410 (1999).

[3] B. A. Paldus and A. A. Kachanov, "An historical overview of cavity-enhanced methods," Can. J. Phys. **83**, 975–999 (2005).

[4] K. L. Bechtel, R. N. Zare, A. A. Kachanov, S. S. Sanders, and B. A. Paldus, "Moving beyond traditional UV-visible absorption detection: cavity ring-down spectroscopy for HPLC," Anal. Chem. **77**, 1177–1182 (2005).

[5] A. M. Shaw, T. E. Hannon, F. Li, and R. N. Zare, "Adsorption of crystal violet to the silica-water interface monitored by evanescent wave cavity ring-down spectroscopy," J. Phys. Chem. B **107**, 7070–7075 (2003).

[6] A. C. R. Pipino, J. W. Hudgens, and R. E. Huie, "Evanescent wave cavity ring-down spectroscopy with a total-internal-reflection minicavity," Rev. Sci. Instrum. **68**, 2978–2989 (1997).

[7] P. B. Tarsa, D. M. Brzozowski, P. Rabinowitz, and K. K. Lehmann, "Cavity ringdown strain gauge," Opt. Lett. **29**, 1339–1341 (2004).

[8] G. Berden, R. Peeters, and G. Meijer, "Cavity ring-down spectroscopy: Experimental schemes and applications," Int. Rev. Phys. Chem. **19**, 565–607 (2000).

[9] H. Naus, I. H. M. van Stokkum, W. Hogervorst, and W. Ubachs, "Quantitative analysis of decay transients applied to a multimode pulsed cavity ringdown experiment," Appl. Opt. **40**, 4416–4426 (2001).

[10] J. Y. Lee, H.-W. Lee, J. W. Kim, Y. S. Yoo, and J. W. Hahn, "Measurement of ultralow supermirror birefringence by use of the polarimetric differential cavity ringdown technique," Appl. Opt. **39**, 1941–1945 (2000).

[11] M. W. Chbat, P. A. Perrier, and P. R. Prucnal, "Optical clock recovery demonstration using periodic oscillations of a hybrid electrooptic bistable system," IEEE Photon. Technol. Lett. **3**, 65–67 (1991).

[12] M. Jinno and T. Matsumoto, "All-optical timing extraction using 1.5 μm self pulsating multielectrode DFB LD," Electron. Lett. **24**, 1426–1427 (1988).

[13] M. Jinno, T. Matsumoto, and M. Koga, "All-optical timing extraction using an optical tank circuit," IEEE Photon. Technol. Lett. **2**, 203–204 (1990).

[14] E. Kehayas, L. Stampoulidis, H. Avramopoulos, Y. Liu, E. Tangdiongga, and H. J. S. Dorren, "40 Gb/s all-optical packet clock recovery with ultrafast lock-in time and low inter-packet guardbands," Opt. Express **13**, 475–480 (2005).

[15] D. L. Butler, J. S. Wey, M. W. Chbat, G. L. Burdge, and J. Goldhar, "Optical clock recovery from a data stream of an arbitrary bit rate by use of stimulated Brillouin scattering," Opt. Lett. **20**, 560–562 (1995).

[16] J. Lee, H. Cho, S. K. Lim, S. S. Lee, and J. S. Ko, "Optical clock recovery scheme for a high bit rate nonreturn-to-zero signal using fiber Bragg grating filters," Opt. Eng. **44**, 020,502 (2005).

[17] X. Zhou, C. Lu, P. Shum, H. H. M. Shalaby, T. H. Cheng, and P. Ye, "A performance analysis of an all-optical clock extraction circuit based on Fabry-Perot filter," J. Lightw. Technol. **19**, 603–613 (2001).

[18] C. Johnson, K. Demarest, C. Allen, R. Hui, K. V. Peddanarappagari, and B. Zhu, "Multiwavelength all-optical clock recovery," IEEE Photon. Technol. Lett. **11**, 895–897 (1999).

[19] D. V. Kuksenkov, S. Li, M. Sauer, and D. A. Nolan, "Mo3.5.1 Nonlinear fibre devices operating on multiple WDM channels," in *31st European Conference on Optical Communication*, pp. 51–54 (The Institution of Electrical Engineers, London, 2005).

[20] V. Mikhailov and P. Bayvel, "All-optical multiwavelength clock recovery using integrated semiconductor amplifier array module," Electron. Lett. **37**, 232–234 (2001).

[21] B. Lee, "Review of the present status of optical fiber sensors," Opt. Fiber Technol. **9**, 57–79 (2003).

[22] A. Othonos, "Fiber Bragg gratings," Rev. Sci. Instrum. **68**, 4309–4341 (1997).

[23] P. Urquhart, "Review of rare earth doped fibre lasers and amplifiers," IEE Proc. **135**, 385–407 (1988).

[24] N. Hodgson and H. Weber, *Optical Resonators* (Springer-Verlag, 1997).

[25] J. F. Mulligan, "Who were Fabry and Pérot?" Am. J. Phys. **66**, 797–802 (1998).

[26] D. K. Armani, T. J. Kippenberg, S. M. Spillane, and K. J. Vahala, "Ultra-high-Q toroid microcavity on a chip," Nature **421**, 925–928 (2003).

[27] J. J. Scherer, J. B. Paul, A. O'Keefe, and R. J. Saykally, "Cavity ringdown laser absorption spectroscopy: history, development, and application to pulsed molecular beams," Chem. Rev. **97**, 25–51 (1997).

[28] T. Lerber and A. Romann, "Fiber optic sensor with an optical resonator," European Patent Application EP1195582 (2002).

[29] J. M. Herbelin, J. A. McKay, M. A. Kwok, R. H. Uenten, D. S. Urevig, D. J. Spencer, and D. J. Benard, "Sensitive measurement of photon lifetime and true reflectances in an optical cavity by a phase-shift method," Appl. Opt. **19**, 144–147 (1980).

[30] D. Z. Anderson, J. C. Frisch, and C. S. Masser, "Mirror reflectometer based on optical cavity decay time," Appl. Opt. **23**, 1238–1245 (1984).

[31] A. O'Keefe and D. A. Deacon, "Cavity ring-down optical spectrometer for absorption measurements using pulsed laser sources," Rev. Sci. Instrum. **59**, 2544–2551 (1988).

[32] R. T. Jongma, M. G. H. Boogaarts, I. Holleman, and G. Meijer, "Trace gas detection with cavity ring down spectroscopy," Rev. Sci. Instrum. **66**, 2821–2828 (1995).

[33] R. Engeln and G. Meijer, "A Fourier transform cavity ring down spectrometer," Rev. Sci. Instrum. **67**, 2708–2713 (1996).

[34] J. T. Hodges, J. P. Looney, and R. D. van Zee, "Response of a ring-down cavity to an arbitrary excitation," J. Chem. Phys. **105**, 10,278–10,289 (1996).

[35] D. Romanini, A. A. Kachanov, N. Sadeghi, and F. Stoeckel, "CW cavity ring down spectroscopy," Chem. Phys. Lett. **264**, 316–322 (1997).

[36] J. W. Hahn, Y. S. Yoo, J. Y. Lee, J. W. Kim, and H.-W. Lee, "Cavity ringdown spectroscopy with a continuous-wave laser: calculation of coupling efficiency and a new spectrometer design," Appl. Opt. **38**, 1859–1866 (1999).

[37] Y. He and B. J. Orr, "Continuous-wave cavity ringdown absorption spectroscopy with a swept-frequency laser: rapid spectral sensing of gas-phase molecules," Appl. Opt. **44**, 6752–6761 (2005).

[38] J. T. Hodges, J. P. Looney, and R. D. van Zee, "Laser bandwidth effects in quantitative cavity ring-down spectroscopy," Appl. Opt. **35**, 4112–4116 (1996).

[39] K. K. Lehmann and D. Romanini, "The superposition principle and cavity ring-down spectroscopy," J. Chem. Phys. **105**, 10,263–10,277 (1996).

[40] M. Jakubinek, Z. Tong, S. Manzhos, and H.-P. Loock, "Configuration of ring-down spectrometers for maximum sensitivity," Can. J. Chem. **82**, 873–879 (2004).

[41] A. C. R. Pipino, "Monolithic folded resonator for evanescent wave cavity ringdown spectroscopy," Appl. Opt. **39**, 1449–1453 (2000).

[42] A. C. R. Pipino, J. P. M. Hoefnagels, and N. Watanabe, "Absolute surface coverage measurement using a vibrational overtone," J. Chem. Phys. **120**, 2879–2888 (2004).

[43] T. E. Hannon, S. Chah, and R. N. Zare, "Evanescent-wave cavity ring-down investigation of polymer/solvent interactions," J. Phys. Chem. B **109**, 7435–7442 (2005).

[44] P. R. Morkel, M. C. Farries, and D. N. Payne, "Losses in fibre laser cavities," Electron. Lett. **24**, 92–93 (1988).

[45] G. Stewart, K. Atherton, H. Yu, and B. Culshaw, "An investigation of an optical fibre amplifier loop for intra-cavity and ring-down cavity loss measurements," Meas. Sci. Technol. **12**, 843–849 (2001).

[46] M. Gupta, H. Jiao, and A. O'Keefe, "Cavity-enhanced spectroscopy in optical fibers," Opt. Lett. **27**, 1878–1880 (2002).

[47] G. Stewart, P. Shields, and B. Culshaw, "Development of fibre laser systems for ring-down and intracavity gas spectroscopy in the near-IR," Meas. Sci. Technol. **15**, 1621–1628 (2004).

[48] G. Stewart, K. Atherton, and B. Culshaw, "Cavity-enhanced spectroscopy in fiber cavities," Opt. Lett. **29**, 442–444 (2004).

[49] R. S. Brown, I. Kozin, Z. Tong, R. D. Oleschuk, and H.-P. Loock, "Fiber-loop ring-down spectroscopy," J. Chem. Phys. **117**, 10,444–10,447 (2002).

[50] P. B. Tarsa, A. D. Wist, P. Rabinowitz, and K. K. Lehmann, "Single-cell detection by cavity ring-down spectroscopy," Appl. Phys. Lett. **85**, 4523–4525 (2004).

[51] P. B. Tarsa, P. Rabinowitz, and K. K. Lehmann, "Evanescent field absorption in a passive optical fiber resonator using continuous-wave cavity ring-down spectroscopy," Chem. Phys. Lett. **383**, 297–303 (2004).

[52] D. E. Vogler, M. G. Müller, and M. W. Sigrist, "Fiber-optic cavity sensing of hydrogen diffusion," Appl. Opt. **42**, 5413–5417 (2003).

[53] D. E. Vogler, A. Lorencak, J. M. Rey, and M. W. Sigrist, "Bending loss measurement using a fiber cavity ringdown scheme," Opt. Laser Eng. **43**, 527–535 (2005).

[54] C. Wang and S. T. Scherrer, "Fiber loop ringdown for physical sensor development: pressure sensor," Appl. Opt. **43**, 6458–6464 (2004).

[55] C. Wang and S. T. Scherrer, "Fiber ringdown pressure sensors," Opt. Lett. **29**, 352–354 (2004).

[56] R. Engeln, G. Berden, E. van den Berg, and G. Meijer, "Polarization dependent cavity ring down spectroscopy," J. Chem. Phys. **107**, 4458–4467 (1997).

[57] F. Maystre and R. Dandliker, "Polarimetric fiber optical sensor with high sensitivity using a Fabry-Perot structure," Appl. Opt. **28**, 1995–2000 (1989).

[58] P. Rabinowitz and K. Lehmann, "System and method of data reduction for improved exponential decay measurements," US Patent 6915240 (2006).

[59] C. Roslund and C. Beckman, "Disputing Viking navigation by polarized skylight," Appl. Opt. **33**, 4754–4755 (1994).

[60] H. Kubbinga, "Christiaan Huygens and the foundations of optics," Pure Appl. Opt. **4**, 723–739 (1995).

[61] W. Heisenberg and H. Euler, "Folgerungen aus der Diracschen Theorie des Positrons," Z. Phys. **98**, 714–732 (1936).

[62] R. Ulrich and A. Simon, "Polarization optics of twisted single-mode fibers," Appl. Opt. **18**, 2241–2251 (1979).

[63] T. Chartier, A. Hideur, C. Özkul, F. Sanchez, and G. M. Stéphan, "Measurement of the elliptical birefringence of single-mode optical fibers," Appl. Opt. **40**, 5343–5353 (2001).

[64] H. Y. Kim, E. H. Lee, and B. Y. Kim, "Polarization properties of fiber lasers with twist-induced circular birefringence," Appl. Opt. **36**, 6764–6769 (1997).

[65] C. Rizzo, A. Rizzo, and D. M. Bishop, "The Cotton-Mouton effect in gases: experiment and theory," Int. Rev. in Phys. Chem. **16**, 81–111 (1997).

[66] E. Zavattini, G. Zavattini, G. Ruoso, E. Polacco, E. Milotti, M. Karuza, U. Gastaldi, G. D. Domenico, F. D. Valle, R. Cimino, S. Carusotto, G. Cantatore, and M. Bregant, "Experimental observation of optical rotation generated in vacuum by a magnetic field," Phys. Rev. Lett. **96**, 110,406 (2006).

[67] S. Moriwaki, H. Sakaida, T. Yuzawa, and N. Mio, "Measurement of the residual birefringence of interferential mirrors using Fabry-Perot cavity," Appl. Phys. B **65**, 347–350 (1997).

[68] J. L. Hall, J. Ye, and L.-S. Ma, "Measurement of mirror birefringence at the sub-ppm level: proposed application to a test of QED," Phys. Rev. A **62**, 013,815 (2000).

[69] J. Morville and D. Romanini, "Sensitive birefringence measurement in a high-finesse resonator using diode laser optical self-locking," Appl. Phys. B **74**, 495–501 (2002).

[70] S. Rashleigh, "Origins and control of polarization effects in signle-mode fibers," J. Lightw. Technol. **1**, 312–331 (1983).

[71] E. A. Kuzin, J. M. Estudillo, B. I. Escamilla, and J. W. Haus, "Measurements of beat length in short low-birefringence fibers," Opt. Lett. **26**, 1134–1136 (2001).

[72] D. Cotter and A. D. Ellis, "Asynchronous digital optical regeneration and networks," J. Lightw. Technol. **16**, 2068–2080 (1998).

[73] S. A. Hamilton, B. S. Robinson, T. E. Murphy, S. J. Savage, and E. P. Ippen, "100 Gb/s optical time-division multiplexed networks," J. Lightw. Technol. **20**, 2086–2100 (2002).

[74] O. Leclerc, B. Lavigne, E. Balmefrezol, P. Brindel, L. Pierre, D. Rouvillain, and F. Seguineau, "Optical regeneration at 40 Gb/s and beyond," J. Lightw. Technol. **21**, 2779–2790 (2003).

[75] K. Vlachos, N. Pleros, C. Bintjas, G. Theophilopoulos, and H. Avramopoulos, "Ultrafast time-domain technology and its application in all-optical signal processing," J. Lightw. Technol. **21**, 1857–1868 (2003).

[76] M. Saruwatari, "All-optical signal processing for terabit/second optical transmission," IEEE J. Sel. Top. Quantum Electron. **6**, 1363–1374 (2000).

[77] S. Kawanishi and M. Saruwatari, "New-type phase-locked loop using travelling-wave laser-diode optical amplifier for very high-speed optical transmission," Electron. Lett. **24**, 1452–1453 (1988).

[78] S. Kawanishi and M. Saruwatari, "10 GHz timing extraction from randomly modulated optical pulses using phase-locked loop with travelling-wave laser-diode optical amplifier using optical gain modulation," Electron. Lett. **28**, 510–511 (1992).

[79] S. Kawanishi and M. Saruwatari, "Ultra-high-speed PLL-type clock recovery circuit based on all-optical gain modulation in traveling-wave laser diode amplifier," J. Lightw. Technol. **11**, 2123–2129 (1993).

[80] E. S. Awad, C. J. K. Richardson, P. S. Cho, N. Moulton, and J. Goldhar, "Optical clock recovery using SOA for relative timing extraction between counterpropagating short picosecond pulses," IEEE Photon. Technol. Lett. **14**, 396–398 (2002).

[81] H. Bülow, "Optoelectronic synchronization scheme for ultrahigh-speed optical demultiplexer," Electron. Lett. **31**, 1937–1938 (1995).

[82] I. D. Phillips, A. Gloag, P. N. Kean, N. J. Doran, I. Bennion, and A. D. Ellis, "Simultaneous demultiplexing, data regeneration, and clock recovery with a single semiconductor optical amplifier-based nonlinear-optical loop mirror," Opt. Lett. **22**, 1326–1328 (1997).

[83] T. Yamamoto, L. Oxenløwe, C. Schmidt, C. Schubert, E. Hilliger, U. Feiste, J. Berger, R. Ludwig, and H. G. Weber, "Clock recovery from 160 Gbit/s data signals using phase-locked loop with interferometric optical switch based on semiconductor optical amplifier," Electron. Lett. **37**, 509–510 (2001).

[84] Y. M. Jhon, H. J. Ki, and S. H. Kim, "Clock recovery from 40 Gbps optical signal with optical phase-locked loop based on a terahertz optical asymmetric demultiplexer," Opt. Commun. **220**, 315–319 (2003).

[85] I. D. Phillips, A. Gloag, D. G. Moodie, N. J. Doran, I. Bennion, and A. D. Ellis, "Simultaneous demultiplexing and clock recovery using a single electroabsorption modulator in a novel bi-directional configuration," Opt. Commun. **150**, 101–105 (1998).

[86] I. D. Phillips, A. Gloag, D. G. Moodie, N. J. Doran, I. Bennion, and A. D. Ellis, "Drop and insert multiplexing with simultaneous clock recovery using an electroabsorption modulator," IEEE Photon. Technol. Lett. **10**, 291–293 (1998).

[87] D. T. K. Tong, B. Mikkelsen, G. Raybon, T. N. Nielsen, K. F. Dreyer, and J. E. Johnson, "Opto-electronic phase-locked loop with balanced photodetection for clock recovery in high-speed optical time-division-multiplexed systems," IEEE Photon. Technol. Lett. **12**, 1064–1066 (2000).

[88] D. T. K. Tong, K. Deng, B. Mikkelsen, G. Raybon, K. F. Dreyer, and J. E. Johnson, "160 Gbit/s clock recovery using electroabsorption modulator-based phase-locked loop," Electron. Lett. **36**, 1951–1952 (2000).

[89] I. Kang and M. Yan, "Simple setup for simultaneous optical clock recovery and ultra-short sampling pulse generation," Electron. Lett. **38**, 1199–1201 (2002).

[90] C. Boerner, C. Schubert, C. Schmidt, E. Hilliger, V. Marembert, J. Berger, S. Ferber, E. Dietrich, R. Ludwig, B. Schmauss, and H. G. Weber, "160 Gbit/s clock recovery with electrooptical PLL using bidirectionally operated electroabsorption modulator as phase comparator," Electron. Lett. **39**, 1071–1073 (2003).

[91] J. P. Turkiewicz, E. Tangdiongga, G. D. Khoe, and H. de Waardt, "Clock recovery and demultiplexing performance of 160-Gb/s OTDM field experiments," IEEE Photon. Technol. Lett. **16**, 1555–1557 (2004).

[92] H. Chou, Z. Hu, J. E. Bowers, D. J. Blumenthal, K. Nishimura, R. Inohara, and M. Usami, "Simultaneous 160-Gb/s demultiplexing and clock recovery by utilizing microwave harmonic frequencies in a traveling-wave electroabsorption modulator," IEEE Photon. Technol. Lett. **16**, 608–610 (2004).

[93] E. S. Awad, P. S. Cho, C. Richardson, N. Moulton, and J. Goldhar, "Optical 3R regeneration using a single EAM for all-optical timing extraction with simultaneous reshaping and wavelength conversion," IEEE Photon. Technol. Lett. **14**, 1378–1380 (2002).

[94] E. S. Awad, P. S. Cho, N. Moulton, and J. Goldhar, "All-optical timing extraction with simultaneous optical demultiplexing from 40 Gb/s using a single electroabsorption modulator," IEEE Photon. Technol. Lett. **15**, 126–128 (2003).

[95] E. S. Awad, P. S. Cho, N. Moulton, and J. Goldhar, "Subharmonic optical clock recovery from 160 Gb/s using time-dependent loss saturation inside a single electroabsorption modulator," IEEE Photon. Technol. Lett. **15**, 1764–1766 (2003).

[96] E. S. Awad, P. S. Cho, and J. Goldhar, "Simultaneous four-wave mixing and cross-absorption modulation inside a single EAM for high-speed optical demultiplexing and clock recovery," IEEE Photon. Technol. Lett. **17**, 1534–1536 (2005).

[97] H. Dong, H. Sun, G. Zhu, Q. Wang, and N. K. Dutta, "Clock recovery using cascaded $LiNbO_3$ modulator," Opt. Express **12**, 4751–4757 (2004).

[98] G. Zhu, Q. Wang, H. Dong, H. Sun, and N. K. Dutta, "80Gb/s clock recovery with phase locked loop based on $LiNbO_3$ modulators," Opt. Express **12**, 3488–3492 (2004).

[99] G. Zhu, Q. Wang, H. Chen, and N. K. Dutta, "High-speed clock recovery with phase-locked loop based on $LiNbO_3$ modulators," Opt. Eng. **43**, 1056–1059 (2004).

[100] O. Kamatani, S. Kawanishi, and M. Saruwatari, "Prescaled 6.3 GHz clock recovery from 50 Gbit/s TDM optical signal with 50 GHz PLL using four-wave mixing in a travelling-wave laser diode optical amplifier," Electron. Lett. **30**, 807–809 (1994).

[101] O. Kamatani and S. Kawanishi, "Prescaled timing extraction from 400 Gb/s optical signal using a phase lock loop based on four-wave-mixing in a laser diode amplifier," IEEE Photon. Technol. Lett. **8**, 1094–1096 (1996).

[102] O. Kamatani and S. Kawanishi, "Ultrahigh-speed clock recovery with phase lock loop based on four-wave mixing in a traveling-wave laser diode amplifier," J. Lightw. Technol. **14**, 1757–1767 (1996).

[103] D. H. Kim, S. H. Kim, J. C. Jo, and S. S. Choi, "Ultrahigh-speed clock recovery with optical phase lock loop based on four-wave-mixing in a semiconductor optical amplifier," Opt. Commun. **182**, 329–334 (2000).

[104] M. Hyodo, K. S. Abedin, N. Onodera, and M. Watanabe, "Harmonic synchronization of Fourier-synthesized optical pulses to an external optical clock," IEEE Photon. Technol. Lett. **16**, 281–283 (2004).

[105] R. Salem and T. E. Murphy, "Broad-band optical clock recovery system using two-photon absorption," IEEE Photon. Technol. Lett. **16**, 2141–2143 (2004).

[106] R. Salem, G. E. Tudury, T. U. Horton, G. M. Carter, and T. E. Murphy, "Polarization-insensitive optical clock recovery at 80 Gb/s using a silicon photodiode," IEEE Photon. Technol. Lett. **17**, 1968–1970 (2005).

[107] X. S. Yao and G. Lutes, "A high-speed photonic clock and carrier recovery device," IEEE Photon. Technol. Lett. **8**, 688–690 (1996).

[108] H. Tsuchida and M. Suzuki, "40-Gb/s optical clock recovery using an injection-locked optoelectronic oscillator," IEEE Photon. Technol. Lett. **17**, 211–213 (2005).

[109] H. Tsuchida, "160-Gb/s optical clock recovery using a regeneratively mode-locked laser diode," IEEE Photon. Technol. Lett. **18**, 1687–1689 (2006).

[110] B. Mikkelsen, G. Raybon, R. Essiambre, A. J. Stentz, T. N. Nielsen, D. W. Peckham, L. Hsu, L. Gruner-Nielsen, K. Dreyer, and J. E. Johnson, "320-Gb/s single-channel pseudolinear transmission over 200 km of nonzero-dispersion fiber," IEEE Photon. Technol. Lett. **12**, 1400–1402 (2000).

[111] J. Lasri, P. Devgan, R. Tang, and P. Kumar, "Ultralow timing jitter 40-Gb/s clock recovery using a self-starting optoelectronic oscillator," IEEE Photon. Technol. Lett. **16**, 263–265 (2004).

[112] Z. Hu, H.-F. Chou, J. E. Bowers, and D. J. Blumenthal, "40-Gb/s optical clock recovery using a compact traveling-wave electroabsorption modulator-based ring oscillator," IEEE Photon. Technol. Lett. **16**, 1376–1378 (2004).

[113] Z. Hu, K. Nishimura, H. Chou, L. Rau, M. Usami, J. E. Bowers, and D. J. Blumenthal, "40-Gb/s optical packet clock recovery with simultaneous reshaping using a traveling-wave electroabsorption modulator-based ring oscillator," IEEE Photon. Technol. Lett. **16**, 2640–2642 (2004).

[114] Z. Hu, H.-F. Chou, K. Nishimura, M. Usami, J. E. Bowers, and D. J. Blumenthal, "Optical clock recovery circuits using traveling-wave electroabsorption modulator-based ring oscillators for 3R regeneration," IEEE J. Sel. Top. Quantum Electron. **11**, 329–337 (2005).

[115] H. Chou, Z. Hu, J. E. Bowers, and D. J. Blumenthal, "Compact optical 3R regeneration using a traveling-wave electroabsorption modulator," IEEE Photon. Technol. Lett. **17**, 486–488 (2005).

[116] T. Miyazaki and F. Kubota, "Simultaneous demultiplexing and clock recovery for 160-Gb/s OTDM signal using a symmetric Mach-Zehnder switch in electrooptic feedback loop," IEEE Photon. Technol. Lett. **15**, 1008–1010 (2003).

[117] P. E. Barnsley, H. J. Wickes, G. E. Wickens, and D. M. Spirit, "All-optical clock recovery from 5 Gb/s RZ data using a self-pulsating 1.56 μm laser diode," IEEE Photon. Technol. Lett. **3**, 942–945 (1991).

[118] P. E. Barnsley, G. E. Wickens, H. J. Wickes, and D. M. Spirit, "A 4 x 5 Gb/s transmission system with all-optical clock recovery," IEEE Photon. Technol. Lett. **4**, 83–86 (1992).

[119] P. E. Barnsley and H. J. Wickes, "All-optical clock recovery from 2.5 Gbit/s NRZ data using selfpulsating 1.58 μm laser diode," Electron. Lett. **28**, 4–6 (1992).

[120] P. E. Barnsley, "NRZ format all-optical clock extraction at 3.2Gbit/s using two-contact semiconductor devices," Electron. Lett. **28**, 1253–1255 (1992).

[121] R. Ludwig and A. Ehrhardt, "Turn-key-ready wavelength-, repetition rate- and pulsewidth-tunable femtosecond hybrid modelocked semiconductor laser," Electron. Lett. **31**, 1165–1167 (1995).

[122] R. Ludwig, A. Ehrhardt, W. Pieper, E. Jahn, N. Agrawal, H.-J. Ehrke, L. Küller, and H. Weber, "40Gbit/s demultiplexing experiment with 10GHz all-optical clock recovery using a modelocked semiconductor laser," Electron. Lett. **32**, 327–329 (1996).

[123] H. Bao, Y. J. Wen, and H.-F. Liu, "Impact of saturable absorption on performance of optical clock recovery using a mode-locked multisection semiconductor laser," IEEE J. Quantum Electron. **40**, 1177–1185 (2004).

[124] S. Arahira, S. Sasaki, K. Tachibana, and Y. Ogawa, "All-optical 160-Gb/s clock extraction with a mode-locked laser diode module," IEEE Photon. Technol. Lett. **16**, 1558–1560 (2004).

[125] T. Ohno, K. Sato, T. Shimizu, T. Furuta, and H. Ito, "Recovery of 40 GHz optical clock from 160 Gbit/s data using regeneratively modelocked semiconductor laser," Electron. Lett. **39**, 453–455 (2003).

[126] T. Ohno, S. Kodama, T. Yoshimatsu, K. Yoshino, and H. Ito, "160 Gbit/s OTDM receiver consisting of PD-EAM optical-gate and MLLD-based optical clock recovery device," Electron. Lett. **40**, 1285–1286 (2004).

[127] T. Ohno, K. Sato, R. Iga, Y. Kondo, K. Yoshino, T. Furuta, and H. Ito, "Recovery of 80 GHz optical clock from 160 Gbit/s data using regeneratively modelocked laser diode," Electron. Lett. **39**, 1398–1400 (2003).

[128] T. Ohno, K. Sato, R. Iga, Y. Kondo, T. Ito, T. Furuta, K. Yoshino, and H. Ito, "Recovery of 160 GHz optical clock from 160 Gbit/s data stream using modelocked laser diode," Electron. Lett. **40**, 265–267 (2004).

[129] B. K. Mathason and P. J. Delfyett, "Pulsed injection locking dynamics of passively mode-locked external-cavity semiconductor laser systems for all-optical clock recovery," J. Lightw. Technol. **18**, 1111–1120 (2000).

[130] T. Miyazaki, H. Sotobayashi, and W. Chujo, "Synchronous optical demultiplexing and sampling of 80-Gb/s OTDM signals by optically recovered clock using mode-locked laser diode and symmetric Mach-Zehnder switch," IEEE Photon. Technol. Lett. **14**, 1734–1736 (2002).

[131] M. Möhrle, U. Feiste, J. Hörer, R. Molt, and B. Sartorius, "Gigahertz self-pulsation in 1.5 μm wavelength multisection DFB lasers," IEEE Photon. Technol. Lett. **4**, 976–978 (1992).

[132] D. J. As, R. Eggemann, U. Feiste, M. Möhrle, E. Patzak, and K. Weich, "Clock recovery based on a new type of self-pulsation in a 1.5 μm two-section InGaAsP/InP DFB laser," Electron. Lett. **29**, 141–142 (1993).

[133] U. Feiste, D. J. As, and A. Ehrhardt, "18 GHz all-optical frequency locking and clock recovery using a self-pulsating two-section DFB-laser," IEEE Photon. Technol. Lett. **6**, 106–108 (1994).

[134] W. Mao, Y. Li, M. Al-Mumin, and G. Li, "40 Gbit/s all-optical clock recovery using two-section gain-coupled DFB laser and semiconductor optical amplifier," Electron. Lett. **37**, 1302–1303 (2001).

[135] W. Mao, Y. Li, M. Al-Mumin, and G. Li, "All-optical clock recovery from RZ-format data by using a two-section gain-coupled DFB laser," J. Lightw. Technol. **20**, 1705–1714 (2002).

[136] Y. Li and G. Li, "80 Gbit/s all-optical clock recovery using two-section gain-coupled DFB laser," Electron. Lett. **38**, 892–893 (2002).

[137] Y. Li, C. Kim, G. Li, Y. Kaneko, R. L. Jungerman, and O. Buccafusca, "Wavelength and polarization insensitive all-optical clock recovery from 96-Gb/s data by using a two-section gain-coupled DFB laser," IEEE Photon. Technol. Lett. **15**, 590–592 (2003).

[138] X. Wang, G. Li, J. Hong, and S. A. Pappert, "Spatiotemporal dynamics and high-frequency self-pulsations in two-section distributed feedback lasers," J. Opt. Soc. Am. B **16**, 2030–2039 (1999).

[139] I. Kim, C. Kim, P. L. LiKamWa, and G. Li, "Dynamics of all-optical clock recovery using two-section index- and gain-coupled DFB lasers," J. Lightw. Technol. **23**, 1704–1712 (2005).

[140] B. Sartorius, M. Möhrle, S. Malchow, and S. Reichenbacher, "Wavelength and polarisation independent all optical synchronisation of high frequency DFB type self-pulsations," Electron. Lett. **32**, 1026–1028 (1996).

[141] B. Sartorius, C. Bornholdt, O. Brox, H. J. Ehrke, D. Hoffmann, R. Ludwig, and M. Möhrle, "All-optical clock recovery module based on self-pulsating DFB laser," Electron. Lett. **34**, 1664–1665 (1998).

[142] B. Sartorius, C. Bornholdt, O. Brox, M. Möhrle, P. Brindel, O. Leclerc, and E. Desurvire, "Analysis and compression of pulses emitted from an all-optical clock recovery modue," Electron. Lett. **34**, 2344–2345 (1998).

[143] C. Bornholdt, B. Sartorius, S. Schelhase, M. Möhrle, and S. Bauer, "Self-pulsating DFB laser for all-optical clock recovery at 40Gbit/s," Electron. Lett. **36**, 327–328 (2000).

[144] I. Monfils, C. Ito, and J. C. Cartledge, "10 Gbit/s all-optical clock recovery using three-section DFB laser with optical feedback," Electron. Lett. **41**, 1342–1343 (2005).

[145] Y. A. Leem, D. Yee, E. Sim, S. Kim, D. C. Kim, and K. H. Park, "Self-pulsation in multisection laser diodes with a DFB reflector," IEEE Photon. Technol. Lett. **18**, 622–624 (2006).

[146] I. Kim, C. Kim, G. Li, P. LiKamWa, and J. Hong, "180-GHz clock recovery using a multisection gain-coupled distributed feedback laser," IEEE Photon. Technol. Lett. **17**, 1295–1297 (2005).

[147] Y. J. Wen, H. F. Liu, D. Novak, and A. Nirmalathas, "All-optical clock recovery at line rate by narrow-band resonant modulation of a single-mode laser diode," IEEE Photon. Technol. Lett. **14**, 1731–1733 (2002).

[148] Y. J. Wen, C.-J. Chae, and H. F. Liu, "Time-domain polarization interleaving of signal to allow polarization-insensitive all-optical clock recovery," IEEE Photon. Technol. Lett. **17**, 1304–1306 (2005).

[149] Y. Yang, Y. J. Wen, A. Nirmalathas, H. F. Liu, and D. Novak, "Optical clock recovery at line rates via injection locking of a long cavity Fabry-Pérot laser diode," IEEE Photon. Technol. Lett. **16**, 1561–1563 (2004).

[150] J. Renaudier, B. Lavigne, F. Lelarge, M. Jourdran, B. Dagens, O. Legouezigou, P. Gallion, and G. Duan, "Standard-compliant jitter transfer function of all-optical clock recovery at 40 GHz based on a quantum-dot self-pulsating semiconductor laser," IEEE Photon. Technol. Lett. **18**, 1249–1251 (2006).

[151] K. Smith and J. K. Lucek, "All-optical clock recovery using a mode-locked laser," Electron. Lett. **28**, 1814–1816 (1992).

[152] A. D. Ellis, K. Smith, and D. M. Patrick, "All optical clock recovery at bit rates up to 40Gbit/s," Electron. Lett. **29**, 1323–1324 (1993).

[153] S. Bigo and E. Desurvire, "20GHz all-optical clock recovery based on fibre laser mode-locking with fibre nonlinear loop mirror as variable intensity/phase modulator," Electron. Lett. **31**, 1855–1857 (1995).

[154] D. Patrick and R. Manning, "20Gbit/s all-optical clock recovery using semiconductor nonlinearity," Electron. Lett. **30**, 151–152 (1994).

[155] S. Bigo, O. Leclerc, P. Brindel, G. Vendrôme, E. Desurvire, P. Doussiére, and T. Ducellier, "All-optical regenerator for 20 Gbit/s transoceanic transmission," Electron. Lett. **33**, 975–976 (1997).

[156] S. Bigo, O. Leclerc, and E. Desurvire, "All-optical fiber signal processing and regeneration for soliton communications," IEEE J. Sel. Top. Quantum Electron. **3**, 1208–1223 (1997).

[157] K. Vlachos, G. Theophilopoulos, A. Hatziefremidis, and H. Avramopoulos, "30 Gb/s all-optical clock recovery circuit," IEEE Photon. Technol. Lett. **12**, 705–707 (2000).

[158] K. G. Vlachos, "Optical clock recovery and clock division at 20 Gb/s using a tunable semiconductor fiber ring laser," Opt. Commun. **222**, 249–255 (2003).

[159] J. He and K. T. Chan, "Wavelength-switchable all optical clock recovery at 10Gbit/s based on semiconductor fiber ring laser," Opt. Express **13**, 327–335 (2005).

[160] T. Wang, Z. Li, C. Lou, Y. Wu, and Y. Gao, "Comb-like filter preprocessing to reduce the pattern effect in the clock recovery based on SOA," IEEE Photon. Technol. Lett. **14**, 855–857 (2002).

[161] L. Yin, G. Liu, J. Wu, and J. Lin, "Reduction of pattern effect for clock recovery based on semiconductor optical amplifier using cw assist light," Opt. Eng. **45**, 045,001 (2006).

[162] T. Wang, C. Lou, L. Huo, Z. Wang, and Y. Gao, "Combination of comb-like filter and SOA for preprocessing to reduce the patten effect in the clock recovery," IEEE Photon. Technol. Lett. **16**, 614–616 (2004).

[163] E. Tangdiongga, J. P. Turkiewicz, G. D. Khoe, and H. de Waardt, "Clock recovery by a fiber ring laser employing a linear optical amplifier," IEEE Photon. Technol. Lett. **16**, 611–613 (2004).

[164] Y. Su, L. Wang, A. Agarwal, and P. Kumar, "Wavelength-tunable all-optical clock recovery using a fiberoptic parametric oscillator," Opt. Commun. **184**, 151–156 (2000).

[165] Z. Wang, T. Wang, C. Lou, L. Huo, and Y. Gao, "A novel approach for clock recovery without pattern effect from degraded signal," Opt. Commun. **219**, 301–306 (2003).

[166] L. E. Adams, E. S. Kintzer, and J. G. Fujimoto, "All-optical clock recovery using a modelocked figure eight laser with a semiconductor nonlinearity," Electron. Lett. **30**, 1696–1697 (1994).

[167] L. E. Adams, E. S. Kintzer, and J. G. Fujimoto, "Performance and scalability of an all-optical clock recovery figure eight laser," IEEE Photon. Technol. Lett. **8**, 55–57 (1996).

[168] H. K. Lee, C. H. Lee, S. B. Kang, M. Jeon, K. H. Kim, J. T. Ahn, and E. Lee, "All-fibre-optic clock recovery from nonreturn-to-zero format data," Electron. Lett. **34**, 478–480 (1998).

[169] H. J. Lee, H. G. Kim, J. Y. Choi, and H. K. Lee, "All-optical clock recovery from NRZ data with simple NRZ-to-PRZ converter based on self-phase modulation of semiconductor optical amplifier," Electron. Lett. **35**, 989–990 (1999).

[170] H. K. Lee, J. T. Ahn, M. Jeon, K. H. Kim, D. S. Lim, and C. Lee, "All-optical clock recovery from NRZ data of 10 Gb/s," IEEE Photon. Technol. Lett. **11**, 730–732 (1999).

[171] H. J. Lee, J. Y. Choi, and H. G. Kim, "Polarisation-independent, stable, all-optical clock recovery using an SOA/grating filter wavelength converter," Electron. Lett. **35**, 1368–1370 (1999).

[172] H. J. Lee, C. G. Lee, and C. Park, "All-optical frequency multiplication/recovery based on a repetitive pulse intensity matching," Opt. Commun. **198**, 37–40 (2001).

[173] L. Wang, Y. Su, A. Agarwal, and P. Kumar, "Polarization insensitive widely tunable all-optical clock recovery based on AM mode-locking of a fiber ring laser," IEEE Photon. Technol. Lett. **12**, 211–213 (2000).

[174] M. Jinno and T. Matsumoto, "Optical tank circuits used for all-optical timing recovery," IEEE J. Quantum Electron. **28**, 895–900 (1992).

[175] C. Bintjas, K. Yiannopoulos, N. Pleros, G. Theophilopoulos, M. Kalyvas, H. Avramopoulos, and G. Guekos, "Clock recovery circuit for optical packets," IEEE Photon. Technol. Lett. **14**, 1363–1365 (2002).

[176] C. Bintjas, K. Vlachos, N. Pleros, and H. Avramopoulos, "Ultrafast nonlinear interferometer (UNI)-based digital optical circuits and their use in packet switching," J. Lightw. Technol. **21**, 2629–2637 (2003).

[177] N. Pleros, K. Vyrsokinos, C. Bintjas, K. Yiannopoulos, K. Vlachos, H. Avramopoulos, and G. Guekos, "All-optical clock recovery from short asynchronous data packets at 10 Gb/s," IEEE Photon. Technol. Lett. **15**, 1291–1293 (2003).

[178] E. Kehayas, G. T. Kanellos, L. Stampoulidis, D. Tsiokos, N. Pleros, G. Guekos, and H. Avramopoulos, "Packet-format and network-traffic transparent optical signal processing," J. Lightw. Technol. **22**, 2548–2556 (2004).

[179] T. Houbavlis, K. E. Zoiros, M. Kalyvas, G. Theophilopoulos, C. Bintjas, K. Yiannopoulos, N. Pleros, K. Vlachos, H. Avramopoulos, L. Schares, L. Occhi, G. Guekos, J. R. Taylor, S. Hansmann, and W. Miller, "All-optical signal processing and applications within the esprit project DO_ALL," J. Lightw. Technol. **23**, 781–801 (2005).

[180] P. Bakopoulos, D. Tsiokos, O. Zouraraki, H. Avramopoulos, G. Maxwell, and A. Poustie, "Compact all-optical packet clock and data recovery circuit using generic integrated MZI switches," Opt. Express **13**, 6401–6406 (2005).

[181] T. Wang, C. Lou, L. Huo, Z. Wang, and Y. Gao, "A simple method for clock recovery," Opt. Laser Technol. **36**, 613–616 (2004).

[182] G. Contestabile, A. D'Errico, M. Presi, and E. Ciaramella, "40-GHz all-optical clock extraction using a semiconductor-assisted Fabry-Pérot filter," IEEE Photon. Technol. Lett. **16**, 2523–2525 (2004).

[183] Z. Zhu, M. Funabashi, Z. Pan, L. Paraschis, and S. J. B. Yoo, "10 000-hop cascaded in-line all-optical 3R regeneration to achieve 1 250 000-km 10-Gb/s transmission," IEEE Photon. Technol. Lett. **18**, 718–720 (2006).

[184] Z. Pan, Z. Zhu, M. Funabashi, H. Yang, and S. J. B. Yoo, "101-hop cascaded operation of an optical-label switching router with all-optical clock recovery and 3R regeneration," IEEE Photon. Technol. Lett. **18**, 1654–1656 (2006).

[185] X. Zhou, H. H. M. Shalaby, L. Chao, T. H. Cheng, and P. Ye, "A performance analysis of all-optical clock extraction circuit based on stimulated Brillouin scattering," J. Lightw. Technol. **18**, 1453–1466 (2000).

[186] J. Lee, H. Cho, and J. S. Ko, "Enhancement of clock component in a nonreturn-to-zero signal through beating process," Opt. Fiber Technol. **12**, 59–70 (2006).

[187] Y. D. Jeong, H. J. Lee, H. Yoo, and Y. H. Won, "All-optical NRZ-to-PRZ converter at 10 Gb/s based on self-phase modulation of Fabry-Perot laser diode," IEEE Photon. Technol. Lett. **16**, 1179–1181 (2004).

[188] G. Contestabile, M. Presi, N. Calabretta, and E. Ciaramella, "All-optical clock recovery from 40 Gbit/s NRZ signal based on clock line enhancement and sharp periodic filtering," Electron. Lett. **40**, 1361–1362 (2004).

[189] W. Mao, M. Al-Mumin, X. Wang, and G. Li, "All-optical enhancement of clock and clock-to-data suppression ratio of NRZ data," IEEE Photon. Technol. Lett. **13**, 239–241 (2001).

[190] W. Mao, Y. Li, M. Al-Mumin, and G. Li, "All-optical clock recovery for both RZ and NRZ data," IEEE Photon. Technol. Lett. **14**, 873–875 (2002).

[191] X. Li, C. Kim, and G. Li, "Wavelength-insensitive all-optical clock extraction and enhancement of nonreturn-to-zero data using a semiconductor optical amplifier and fiber Bragg grating," Opt. Eng. **43**, 2210–2211 (2004).

[192] J. Slovak, C. Bornholdt, J. Kreissl, S. Bauer, M. Biletzke, M. Schlak, and B. Sartorius, "Bit rate and wavelength transparent all-optical clock recovery scheme for NRZ-coded PRBS signals," IEEE Photon. Technol. Lett. **18**, 844–846 (2006).

[193] L. Yin, Y. Yan, Y. Zhou, J. Wu, and J. Lin, "Novel scheme for all-optical clock recovery from NRZ signal," Microw. Opt. Techn. Lett. **48**, 516–521 (2006).

[194] S. Betti, C. Bulli, F. Curti, E. Duca, S. Persia, A. Reale, and G. M. Tosi-Beleffi, "Optical clock recovery from 10-Gb/s NRZ signal," Microw. Opt. Techn. Lett. **42**, 435–437 (2004).

[195] S. Betti, F. Curti, E. Duca, S. Monterosso, A. Reale, and G. M. Tosi-Beleffi, "Optical clock recovery from 10-Gb/s NRZ signal after propagation on 100 km of DS, NZD or SR installed fiber," Microw. Opt. Techn. Lett. **44**, 264–266 (2005).

[196] X. Fan, Z. Xin-Liang, L. Hai-Rong, L. De-Ming, and H. De-Xiu, "Polarization maintaining fibre loop mirror for NRZ-to-PRZ conversion in all-optical clock recovery," Chinese Phys. Lett. **23**, 355–358 (2006).

[197] C.-H. Lee and H. K. Lee, "Passive all-optical clock signal extractor for non-return-to-zero signals," Electron. Lett. **34**, 295–297 (1998).

[198] A. Bilenca, D. Dahan, J. Lasri, and G. Eisenstein, "All-optical processing by fiber delay and four-wave mixing of high-bit-rate nonreturn-to-zero signals for timing extraction by optical injection locking," IEEE Photon. Technol. Lett. **14**, 852–854 (2002).

[199] X. Li, C. Kim, and G. Li, "All-optical passive clock extraction of 40 Gbit/s NRZ data using narrow-band filtering," Opt. Express **12**, 3196–3203 (2004).

[200] C. Kim, I. Kim, X. Li, and G. Li, "All-optical clock recovery of NRZ data at 40 Gbit/s using Fabry-Perot filter and two-section gain-coupled DFB laser," Electron. Lett. **39**, 1456–1458 (2003).

[201] SCHOTT Lithotec AG, "Fused Silica Datasheet," Available at http://www.schott.com/lithotec/english/download/fs_june_2006_final.pdf (2006).

Abstracts of publications

[P1] T. von Lerber and M. W. Sigrist, "Cavity-ring-down principle for fiber-optic resonators: experimental realization of bending loss and evanescent-field sensing," Appl. Opt. **41**, 3567–3575 (2002).

A novel measurement principle for fiber-optic sensing is presented. Use of a cavity-ring-down scheme enables measurements of minute optical losses in high-finesse fiber-optic cavities. The loss may be induced by evanescent-field absorption, fiber bending, fiber degradation, Bragg gratings, or any other effect that might change the fiber transmission or cavity reflector properties. The principle is proved to be rather insensitive to ambient perturbations such as temperature changes. A high-sensitivity measurement of loss due to bending is presented as a proof-of-principle. With a cavity finesse of 627 a sensitivity for induced loss of 108 ppm (4.68×10^{-4} dB) is achieved. Preliminary measurements of evanescent-field absorption are also discussed.

[P2] T. von Lerber and M. W. Sigrist, "Time constant extraction from noisy cavity ring-down signals," Chem. Phys. Lett. **353**, 131–137 (2002).

A new efficient algorithm for the extraction of time constants from exponentially decaying signals is presented. The method is based on a non-linear Newton fitting and it is demonstrated to yield significantly more accurate results than the commonly used weighted least square method under noisy signal conditions. Methods are compared by simulated and true experimental data obtained by a fiber cavity ring-down setup.

[P3] T. von Lerber, H. Ludvigsen, and A. Romann, "Resonator based measurement technique for quantification of minute birefringence," Opt. Express **12**, 1363–1371 (2004).

We present a new method for quantification of minute birefringence in high-finesse resonators. The method is based on observing the homodyne polarization mode beat at the output of the resonator. We show that the mode beat is generated by a phase mismatch of a polarization mode in the cavity and that the magnitude of the birefringence is proportional to the beat frequency. We demonstrate the sensitivity of the technique by measuring polarization properties of a twisted 0.275 m long single-mode fiber cavity. Maximum beat length of the fiber was found to be 10.6 m, which is almost 40 times longer than the length of the studied fiber.

[P4] T. von Lerber, J. Tuominen, H. Ludvigsen, S. Honkanen, and F. Kueppers, "Multichannel and rate all-optical clock recovery," Phot. Techn. Lett. **18**, 1395–1397 (2006).

We report on a new clock recovery scheme utilizing a birefringent fiber resonator and a polarizer that allows for parallel all-optical processing of multiple channels and rates. It is demonstrated for 21 simultaneous channels, 20 carrying data at 10 Gb/s and one at 40 Gb/s. Earlier demonstrations of multichannel operation have reported four recovered channels at only one single rate.

[P5] T. von Lerber, J. Tuominen, H. Ludvigsen, S. Honkanen, and F. Küppers, "Investigation of multiwavelength clock recovery based on heterodyne beats of sideband-filtered signal," Opt. Comm. **271**, 87–90 (2007).

We investigate a new parallel all-optical clock recovery scheme based on heterodyne beats of an optical sideband-filtered signal. The oscillating clock signal is recovered when the filtered sideband is combined with a stable local oscillator. The filtering is performed with an optical resonator, which by nature provides possibility for multiwavelength operation. The local oscillator could be realized by a multiwavelength laser, whose emission wavelengths are injection seeded with carrier wavelengths of the input data. The output signal of such a configuration benefits from a reduced bit-pattern effect and a stable offset level. The sideband filtering is demonstrated for 23 simultaneous channels at 100 GHz DWDM grid, each hosting a data stream of 10 Gbit/s.

ISBN 978-951-22-8901-1
ISBN 978-951-22-8902-8 (PDF)
ISSN 1795-2239
ISSN 1795-4584 (PDF)